Characterisation of an optical strain gauge for pantograph applications.

Khanniche, Rachid

University of Wales Swansea

Department of Electrical & Electronic Engineering

Characterisation of an Optical Strain Gauge For Pantograph Applications

BY

Rachid Khanniche

This Thesis is submitted to the University of Wales Swansea in the candidature for the degree of Master of Philosophy

July 2002

ACKNOWLEDGMENTS

I would like to acknowledge with much gratitude and appreciation the guidance and support provided by my supervisor Dr Timothy Davies, who was very helpful and in almost all the time very accessible.

Many thanks to whoever helped me to realise this piece of work, especially Dr McCowen,, Dr Jewell of Mechanical Department and Mr I Evans of Civil Engineering.

I wish also to thank Morganite Electrical Carbon Ltd and Lucas Engineering Company for providing the equipment and components for the project.

Finally, I would like to thank Mr Jeff Mort for his excellent co-operation.

Declaration

This work has not previously been accepted in substance for any degree and is not being concurrently submitted in candidature for any degree.

Signed **Rachid Khanniche**. (candidate)

Date 14-7-02

STATEMENT 1

This thesis is the result of my own investigations, except where otherwise stated. Other sources are acknowledged by footnotes giving explicit references. A bibliography is appended.

Signed **Rachid Khanniche**. (candidate)

Date 14-7-02

STATEMENT 2

I hereby give consent for my thesis, if accepted, to be available for photocopying and for inter-library loan, and for the title and summary to be made available to outside organisations.

Signed **Rachid Khanniche**. (candidate)

Date 14-7-02

DEDICATION

I dedicate this thesis to all my family: my brother Makhlouf and his family, my brother Mohamed Salah and his family, my sister Akila and her family, my sister Hafida and her family, my brother Ali and his family, my sister Nacera and her family, and my sister Rachida and to all my relatives.

I would like to thank my parents for their support, encouragement and all what they have done for me over all my life.

I also dedicate this thesis to all my true friends. I would like to express my gratitude by greatly thanking all the teachers they taught me over all my academic formation. Special thanks to my mathematics teachers.

CONTENT

LIST OF FIGURES

SYMBOLS & ABRIEVIATION

n & n'	Index of refraction
φ_1	Angle of refraction
φ_2	Angle of incidence
φ_c	Critical angle
θ	Acceptance angle
NA	Numerical Aperture
f_n	Normalised frequency of the fundamental mode
γ_R	Raleigh scattering coefficient
λ	Optical wavelength
p	Average photoelastic coefficient
β_C	Isothermal Compressibility
K	Boltzman constant
T_F	Temperature at which the glass reach a state of thermal equilibrium
$\wp$	Transmission loss factor
L	Length of optical fibre
SRS	Stimulated Raman Scattering
SBS	Stimulated Brillouin Scattering
α_{db}	Fibre attenuation
ν	Source bandwidth
d	Fibre Core Diameter
P_R	Threshold optical power relative to Raman scattering
P_B	Threshold optical power relative to Brillouin scattering
R_c	Threshold curvature radius

n_1'	Core refractive index
n_2'	Cladding refractive index
c_1, c_2	Constants
R	Radius of curvature of the fibre bend
T_l	Losses due to lateral offset
D	Lateral offset
ω_0	Spot Size
α	Angular misalignment
$Loss_{fres}$	Loss due to Fresnel reflection
r	Fraction of light reflected at a single interface
E_g	Band gap Energy
$E_x(t)$	Electrical field components along the X axes
$E_y(t)$	Electrical field components along the Y axes
ω	Angular frequency
T	Temperature
T_α	Loss due to angular misalignment
E_{0x}, E_{oy}	The maximum magnitude of the electric field
ε	Phase difference between E_{0x} and E_{oy}
q_e	Electron charge
N	Molecules per unit volume
m_e	Mass of electron
ω_{0j}	Natural frequency
σ_1, σ_2 , σ_3	Principal stresses
n_1, n_2, n_3	Refractive indices along the principal axes

c	Stress optic coefficient
k	Strain optic coefficient
$\varepsilon_1, \varepsilon_2, \varepsilon_3$	Strain optic coefficients along the principal directions
δ	Relative retardation between the two polarisation components
χ	Thickness of the photo-elastic material
I	Light intensity
I_λ	The maximum light intensity
I_{PD1}	Short circuit current of the photodetector 1
I_{PD2}	Short circuit current of the photodetector 2
β	Principal stress direction
$R_{PD1}(\lambda)$	Spectral sensitivity of the photodiode 1
$R_{PD2}(\lambda)$	Spectral sensitivity of the photodiodes 2
CIE	Commission International D'Eclairage
$X(\lambda), Y(\lambda), Z(\lambda)$	Tristimulus functions
$P(\lambda)$	Spectral Power distribution
$\lambda_e(\varepsilon, \lambda)$	Chromatic transfer function (describes the dominant wavelength)
x, y, z	Chromaticity coordinates of a given colour
X_w, Y_w, Z_w	Coordinates of the achromatic point
K_1, K_2, K_3	Constants specific to photodiode 1, 2, and 3 respectively
θ'	Angle formed by the x-axis and the line joining the origin to the point of coordinate (x, y)
Δ	Retardation of the quarter-Wave plate
ADC	Analogue to digital converter
SAR	Successive approximation register
DAC	Digital to analogue converter

V_{ref}	Reference voltage
V_{out}	Output chromatic voltage
G	Gain factor
LSB	Least significant Byte
MSB	Most significant Byte

SUMMARY

An optical strain gauge is developed and characterised for an active pantograph for high-speed electrical trains applications. The pantograph is subjected to a continuous impact forces when it makes contact with the 25 kV overhead AC line. The carbon based pantograph head is susceptible to crack damage due to these impacts

An optical strain gauge based on the photo-elastic effect has been developed to monitor on line the contact force applied to the pantograph. The sensing system exploits the concept of chromatic modulation that can be produced by spectral changes induced by a controlled birefringence. Moreover the chromatic sensing technique is independent of the light intensity and provides total electrical isolation.

The developed optical strain gauge was assessed to evaluate its performance and to find the range of operation. Static, hysterisis, repeatability and dynamic tests were carried out and the results compared to the theory when applicable. In the static test, it was found that the force against dominant wavelength was linear in the range of 0 to 80 N and became progressively non-linear for forces above 80 N, this is in a good agreement with the theory. These tests were carried out several times over a long period of time, and the results showed a good repeatability, although an acceptable degree of hysterisis was noted. Finally the resistance of the optical strain gauge was tested against dynamically varying loads and found that it exhibited a good resistance. These tests proved the suitability of this proposed optical strain gauge for the development of an active pantograph for high-speed electrical trains applications.

CHAPTER 1

INTRODUCTION

1.1- Background of the Project

The background of this project is briefly outlined. The development of an active pantograph system was set-up in collaboration with Morganite Electrical Carbon Ltd and Lucas Ltd. Morganite provided the manufacture of carbon based pantograph pan heads with embedded fibres, Lucas Ltd provided the expertise, manufacture and packaging of the optical fibre subsystem and the University of Wales Swansea developed the overall control system and the analysis and characterisation of the various components of the system as shown in Figure 1.1.

The block diagram of the overall pantograph condition monitoring system is divided into three subsystems, an optical fibre based crack and wear damage detection, an optical fibre sensor based contact force measurement and a Global Positioning System (GPS) based location identification. The optical fibre is used to sense the wear and crack damage when a crack is developed on the carbon material or the wear damage is near to the last layer of carbon material, a control signal will be generated to remove the damaged pan head from the over-head line equipment. At the same time, the system will pin point the location using a GPS. The contact force is also recorded using optical sensing technique. The data can be used to establish the relationship between the contact force (impacts) and crack, contact force and wear damages, as well as how the overhead line system affects the performance of carbon

material. This project concentrates on the evaluation and characterisation of the optical sensor as highlighted in the overall system block diagram of Figure 1.1.

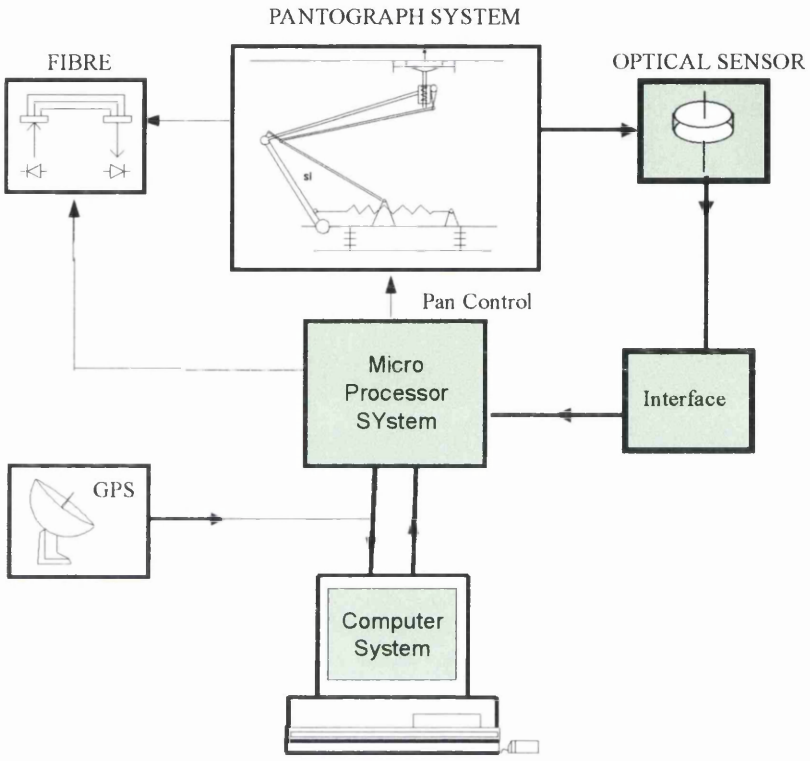

Figure 1.1: Pantograph Mechanism of an Electrified Train

1.2 - Pantographs in High Speed Trains Applications

Pantographs of modern high-speed electrified trains use carbon collector strips to minimise the wear of the overhead wire. However, carbon is susceptible to crack damage due to large impacts from the overhead line, which may result in a total breakdown. The pantograph needs to be kept in contact with the supply AC line at constant pressure to avoid sparking and intermittent loss of power.

Electric railroad vehicles derive their power from an overhead contact wire system, consisting of a pantograph mechanism placed on the roof of the vehicle, which provides current collection. Though this arrangement has been generally satisfactory, the margins of acceptable current collection have been reduced, as the operational speed of vehicles has increased over the years. Moreover, based on the consideration of the capital cost, lighter overhead equipment on the high voltage ac system has been widely used, which adds to the problem. With the increase of speed and the use of the lightweight overhead equipment, dynamic impacts, which directly apply to the carbon material of the pantograph head, has increased dramatically. As a result, crack damage may occur more often on the carbon material, where there are more and larger impacts. The crack, in serious cases, may trap or pull down the overhead line, which has serious consequences for the reliability of an electric train service and operational costs.

1.3 - Project Aims and Objectives

In order to monitor on-line the contact force applied to the pan head, an optical fibre sensor system based upon photo-elastic effect is proposed. The modulation technique consists of producing spectral change that can be induced by a controlled birefringence material subject to the force monitored. To detect the output signal, distimulus detection using two photodiodes having different but overlapping spectral response sensitivities is proposed. This chromatic sensing technique is preferred because it enables intensity insensitive measurement to be made.

This project is concerned with the evaluation and analysis of the optical strain gauge. The optical sensor is to be used to detect the load behaviour experienced by

the electrical pick-ups on the pantograph mechanism of an electrified train as shown in Figure 1.1.

The pantograph is in contact with 25 kV ac supply lines; therefore the optical strain gauge provides a complete immunity to electrical interference and isolation. The conductor wire when it is in contact with the pantograph pick-up may result in large applied forces, for example at the joints in the connector wire and at the suspension points. Little is known about the forces experienced by the pantograph at high speeds.

This work offers a means of quantifying these forces, so that the pantograph pick-up connector wire system can be made more reliable. It also offers a sensor, which could form part of an "active pantograph", designed to minimise the force in the connector wire. Such a system would have the potential to reduce wire on the sliding contact and improve the reliability of high voltage pick-up.

This optical approach to sensing has considerable advantages over other sensing techniques; all stem from the fact that the modulated signal can be transmitted to and from the sensing region without recourse to electrical connection. The main features of this approach are as follow:

- Immunity from electromagnetic interference,
- Electrical isolation, removing problems related to ground plane separation and electrical safety regulation,
- Chemical passivity,
- Small size and low weight,
- A potential high sensitivity and the ability to interface with a wide range of measurands.

Moreover, optical fibres do not generate heat. In addition, optical fibres are low in cost and the dielectric nature of optical fibres makes them compatible with composite materials within which they can be embodied without creating electrical pathways within the structure. These outlined features of an optical fibre sensing system justify the shift towards developing such an optical strain gauge as an alternative to other methods that existed in the last decade.

1.4 - Thesis Layout

The thesis is structured as follows:

Chapter two describes the basic components constituting of an optical fibre sensor and the types of the existing optical fibre sensors. This is followed by a definition of the different criteria upon which the choice of these components for the proposed application is based. Different types of attenuation, which may affect the propagation properties of the light into an optical fibre and the phenomenon of dispersion of the optical signal, their sources and their appropriate remediation, are also discussed in detail. Techniques that can be used to detect the output optical signal are briefly discussed. Finally, notions about the nature of light and its polarisation are introduced to understand better how the current optical sensing system works.

Chapter three describes in details the phenomenon of photo elasticity and its use for strain quantification and distribution.

A practical polariscope, optical system used to determine strain using photo-elastic effect, is discussed. Its fundamental components are defined and the design

criteria upon which the choice of its components are determined and evaluated. Subsequently, a brief overview on the theory of colour measurement is included.

In chapter four the linear detection technique, features and advantages, of the returned optical signal is discussed and evaluated. The last section of this chapter deals with the static and dynamic tests of the optical gauge and the curve of the calibration test is plotted.

The fifth and the last chapter is a final conclusion that can be considered as a brief summary of the content of the thesis and an assessment of the experimental results. A perspective for future work to further improve the assessment of the optical strain gauge for its use in pantograph system is also made.

CHAPTER 2

OPTICAL FIBRE SENSOR SYSTEM

2.1 – Introduction

An optical fibre sensor may be defined as a sensing system in which some constant propagation properties (intensity, phase, state of polarisation...) of an optical signal are modulated in a reproducible and recoverable manner by a measurand [1]. It consists mainly of three components: A light source, an optical fibre and a modulator, Figure 2.1. A light beam generated by an appropriate light source is launched via a coupling mechanism into an optical fibre within which it is guided to the sensing area, where one or more of its aforementioned constant propagation properties may change in a response to the change of the measurand.

At this stage light may exit the transmitting fibre and be modulated in a separate zone before being relaunched into the output fibre. These types of sensors are called **extrinsic.** Such sensors have proved high mechanical stability and flexibility [2]; a typical example of their use is in liquid flow detection and transducers dependent on physical motion. Alternatively, light may be modulated inside the fibre while still guided. Such kinds of sensors [3] are called **intrinsic,** Figure 2.1.

Their main advantage is the reduction of system components, thus reducing signal power losses due to index mismatching between the optical components [4]. Intrinsic sensors are usually used in liquid level detection and displacement.

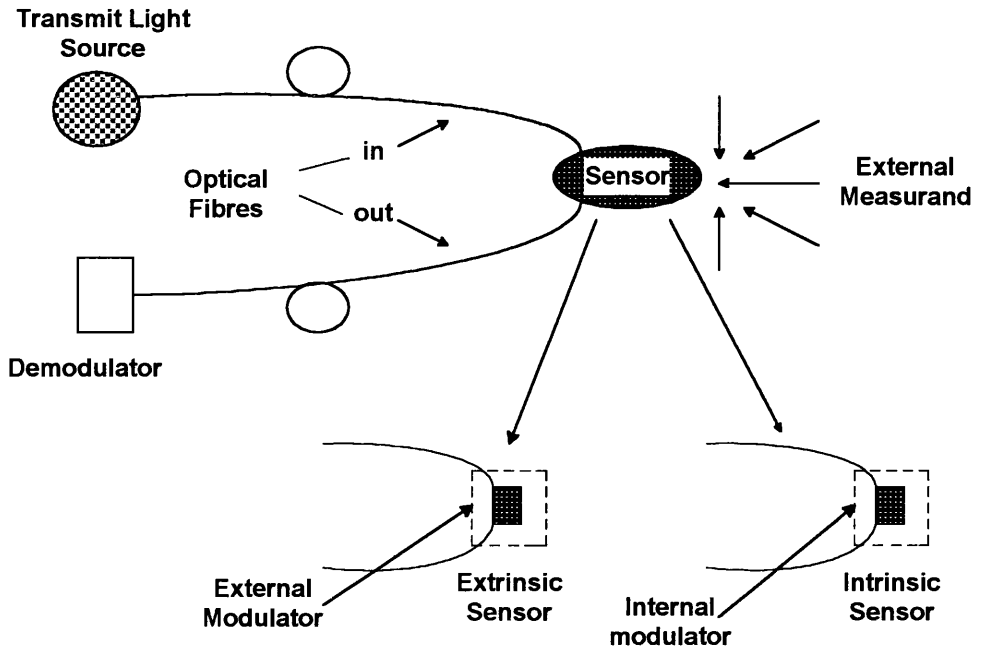

Figure 2.1 - Optical Fibre Sensors System

2.2 - Light Source

The versatility of operating principles, which may exploit an optical fibre sensor, requires a wide range of optical sources to energise these sensor devices. The parameters, which may determine the choice of suitable optical source, are type of the modulation technique used, nature of the signal processing, size and output optical power of the source. There are two types of optical source commonly in use: coherent and non-coherent. For the former class it can distinguish laser sources for example, monomode and multimode lasers, semiconductor lasers, whereas for the latter class LEDs and incandescent sources are relevant examples.

The coherence characteristic of a light source is a measure of the extent to which a phase relationship is maintained across the beam **(spatial coherence)** and along the beam **(temporal coherence)** [2].

2.2.1 - Light Emitting Diode

An LED is basically a forward biased p-n junction; it emits light spontaneously into a wide approximately Lambertian spatial cone [3]. The type of materials, impurities and the doping levels used to form the p-n junction control the band-gap energy, which determines the emitted wavelength, whereas the electric current controls the brightness [5]. As a result of the incoherence characteristic of the emitted light and the large emitting diameter, LEDs are suitable for sensor based upon multimode fibre.

In order to increase the radiance of the LED and to facilitate the coupling with an optical fibre efficiently, hence reducing energy losses, two basic LED structures have been developed; these are surface emitting and edge-emitting LEDs [6].

The surface emitting LED consists of a number of n doped and p doped layers of semiconductor material with a single p-n junction. Light is emitted from a small area perpendicular to the junction where a well is etched to provide an exit path for light [7]. The optical fibre is secured in place with an epoxy resin, Figure 2.2.

By contrast, in the case of the edge emitting LED, light is emitted in the plane of the junction through the edge of the device. This device may be designed with strip geometry, ridge or buried heterostructure. A low emission angle is achieved by the optical guidance of the DH structure. The layers adjacent i.e. the guiding layer must be chosen with a refractive index lower than the index of the active region but higher than the index of the material immediately surrounding it, to maximise the reflection of the radiation into the active area. Furthermore the sides and back of the active region are reflective coated, and the other end-face is anti-reflective coated. Thus, the combination of active and guiding regions forms an asymmetric dielectric wave-guide that channels light towards the fibre core with a fairly high intensity, and allows the

rays to travel in the plane of the junction with much less total absorption loss than they encounter in the active material [8].

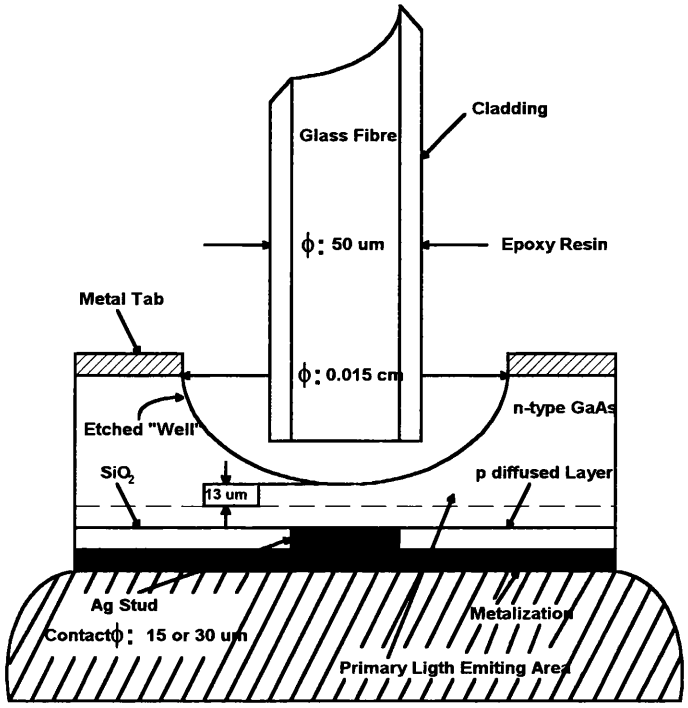

Figure. 2.2 - A DH Surface Emitting LED with Fibre Pig-tail Attached

By suitable choice of matching lens a high launching efficiency of light into an optical fibre can be achieved. Narrowing the active-region has developed a very high radiance edge emitting LED. As much as 0.8 mW has been coupled into a single fibre. The coupling efficiency was further enhanced (by about 3 dB) by the use of a microlens melted onto the fibre end [9].

LEDs acquired high importance within a relatively short time. As a result of the wide range of systems and devices where LEDs can be used, the rate of production was in the order of magnitude of 5×10^9 in 1986 and has increased significantly since. Their use in optical communication is suitable for medium distances up to around 10 km and lower data rates of the order of 100 Mbit/s [10].

The comparison of the capability to launch light into optical fibre of the two structures with respect to their use in high-data-rate fibre-optical communication systems, shows that the edge emitter diode can couple 5 to 6 times more power into low numerical aperture fibres than a surface emitter of the same bandwidth [11].

2.2.2 - Incandescent Source

The heating effect of an electric current flowing through a filament wire causes a collision of atoms which result in transition of electrons from a lower energy level to the higher energy level, and subsequently de-excite spontaneously (i.e. the electrons regain their initial energy levels) with emission of radiation [12, 13]. Since atoms may have several energy levels, a multiplicity of spectral lines of different wavelengths emerges as a continuous spectrum.

Generally, Tungsten is the favoured choice for use as a filament wire, because it has a high melting point and a low rate of evaporation at higher temperature. It emits radiation with an approximate radiance, emitance, excitance, and distribution similar to that of a black-body [14]. Tungsten may operate in vacuum or in an inert gas. The gas is introduced to reduce the evaporation rate of Tungsten from the filament wire, thus, enabling it to be run at high temperatures for long period of life. Moreover, the gas conducts heat away from the filament. Some of the evaporated Tungsten is deposited on the bulb wall causing blackening which affects the brightness of the emitted radiation. However, by adding a halogen to the filling gas, a reversible chemical reaction occurs between the evaporated Tungsten and the halogen. Then the halide Tungsten molecules diffuse towards the filament wire where they dissociate,

the Tungsten is deposited back on the filament while the halogen is available for further reaction.

A typical Tungsten Halogen Lamp (low voltage, with dichroic reflector, 400-1200 nm @ 15W and 12V) has been used to energise the sensor device used in this project [Lucas Engineering]).

2.2.3 - Laser Sources

2.2.3.1 – Laser

The term laser originated as an acronym for Light Amplification by Stimulated Emission of Radiation. The stimulated emission occurs when a stimulating photon falls upon a molecules, or ions, already in the excited state. The incoming photon (stimulating) excites an electron to make a transition to the lower energy level. This transition is accompanied with the emission of a stimulated photon in phase and at the same frequency with the stimulating one. The lazing material can be a solid, gas or liquid. Under condition of thermal equilibrium spontaneous emission is the dominant process and stimulated emission is most unlikely. In order to maximise the rate of stimulated emission the thermal equilibrium condition must be removed to make the higher energy level more populated than the lower ones; this is called **population inversion** and it can be achieved through an excitation process known as **pumping.** Population inversion may be obtained in systems with three or four energy levels. In both systems a metastable state in which atoms spend a long time is obtained.

Three levels system consists of ground energy level and metastable energy level and a higher energy level so that by a suitable pumping mechanism atoms are pumped from the ground level to the higher energy level from where they decay rapidly non-

radiatively either to the ground level or to the metastable level where they spend much time, thus allowing accumulation of a large number of atoms, Figure 2.3. After a short time the number of atoms in the metastable state exceeds those in the ground level and a population inversion is achieved. The stimulated emission takes place between the metastable level and ground level.

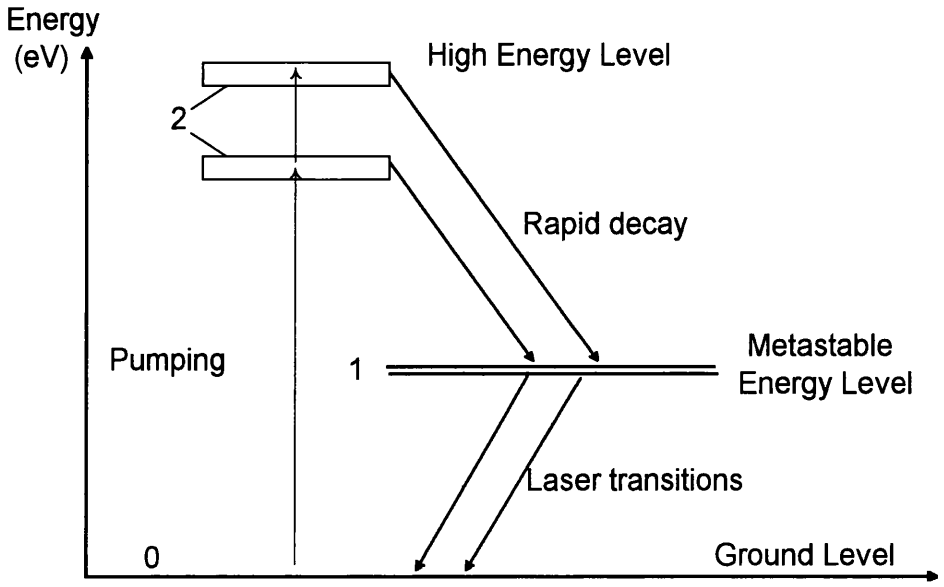

Figure 2.3 - A simplified Schematic Diagram of Three Level Laser

The first ruby laser was based upon three level systems. Three level lasers require an intense burst-pumping source. Moreover, it is difficult to sustain the population inversion, so that this laser operates only in pulsed mode [15].

By contrast, four level systems are characterised by much lower pumping intensity. The excitation energy raises atoms from the ground level to the short-lived highly excited level. Then, they drop quickly to the metastable level. The laser transition takes the atoms to the lower energy level but not, all the way to the ground state, Figure 2.4.

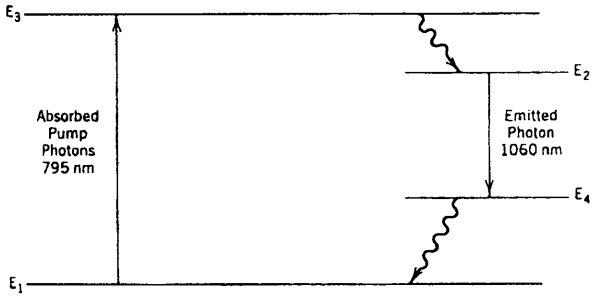

Figure 2.4 - A Simplified Schematic Diagram of Four Level Laser

A typical example of four level systems is the nd : yag laser, which operate in continuous mode [15]. Generally, the gain of a pumped or excited medium is quite small so that the amplification of an optical beam passing once through the medium is minimal [16]. In order to increase the gain, a pair of reflecting mirrors is placed at each end of the medium, so that optical waves may bounce back and forth between the mirrors, until they build up into a coherent and monochromatic laser beam [17]. Moreover when the net laser amplification between mirrors, taking into account any scattering or other losses, exceeds the net reflection loss at the mirrors themselves, then coherent oscillation at optical frequency occurs which results in an emergence of an optical beam whether through a partially transmitting mirror, or by some other technique [18]. This output beam is highly directional and highly monochromatic.

The laser transition may occur between several laser transition levels where each transition corresponds to one wavelength, thus making a laser emitting at different wavelengths. For example, a helium neon laser may emit red wavelength as well as other wavelengths such as yellow, green and orange by suitable optical design.

2.2.3.2 - Laser Diode

A population inversion within a p-n junction may be obtained by heavy doping of both p and n material. When a forward bias approaching the band gap is applied to this device, a stimulated emission takes place near the depletion layer [19]. By putting this device in an optically resonant cavity to provide a feedback the laser action occurs. The resonant cavity may be obtained by polishing the end faces and roughening the sides of the device to preserve the population inversion [3]. To enhance the radiative properties a heterojunction is used and the device is said to have a **heterostructure**. With such a structure radiation confinement to the active region is obtained. However with heterostructure the lazing action takes place across the whole width of the device, which result in unwanted emission through the edge of the device. To overcome this unwanted emission a device with strip geometry has been developed [20]. A strip consists of creation of high resistance areas on either side of the device leaving a small active area for light output. A further, type of optical source exists, namely the glass fibre laser.

2.3 - Optical Fibre

Optical fibre may be defined as a dielectric wave-guide which confines and guides electromagnetic waves by total internal reflection.

It is composed of two different dielectric materials as shown in Figure 2.5. A core with refractive index n'_1 where almost all the energy is confined and it is surrounded by a cladding with refractive index n'_2 where $n'_1 > n'_2$.

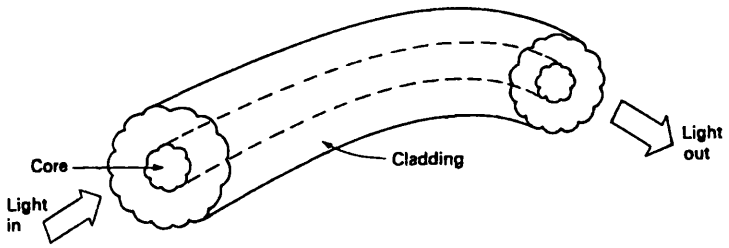

Figure 2.5 - Optical Fibre Wave-Guide Core-Cladding Type

2.3.1 - Propagation of Light Within an Optical Fibre

To understand better the propagation of light in optical fibre the refraction of light at an interface between two dielectrics of differing refractive indices is considered, provided that light is incident on the medium of lower index from the medium of higher index of refraction [19] as shown in Figure 2.6.a.

Snell's law states that the refractive angle φ_1 and the incident angle φ_2 are related by the following equation [19, 21, 22]:

$$n' \sin \varphi_1 = n \sin \varphi_2 \qquad (2.1)$$

Since the ray of light is propagated from the higher density medium to the less dense medium the refractive angle is always greater than that of the incidence. Thus, by increasing the incident angle a case where the refractive angle equal to 90° is achieved and the refractive ray emerges parallel to the interface as shown in Figure 2.6.b. This is known as the limiting case of refraction and the incident angle at which it occurs is known as the **critical angle** φ_c and is given by:

$$\sin \varphi_c = \frac{n}{n'} \qquad (2.2)$$

Increasing further the incident angle, i.e. the incident angle exceeds the critical angle, the light is totally reflected back into the originating medium as shown in Figure 2.6.c.

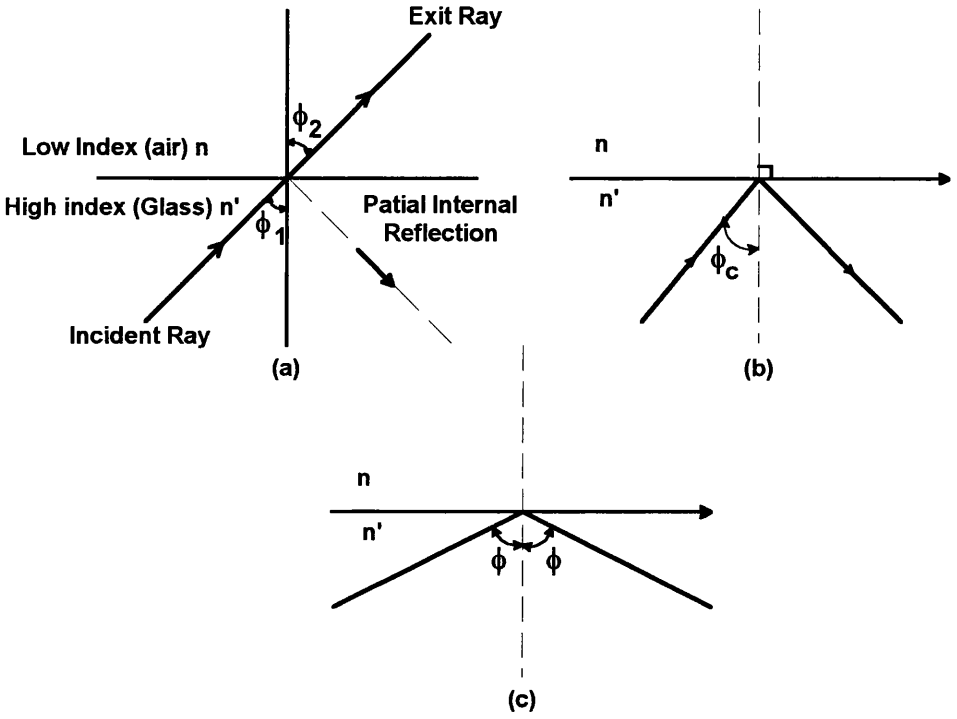

Figure 2.6 - Light Rays Incident on High to Low Interface
(a) Refraction (b) Refraction with Critical Ray at an Angle φ_c
(c) Total Internal Reflection ($\varphi > \varphi_c$)

From the above analysis it is clear that total internal reflection can only occur at an interface between two mediums having different refractive indices when light is incident on the medium of lower refractive index from the medium of higher refractive index at an angle greater than the **critical** angle. This effect of total internal reflection is exploited in optical fibre sensor to trap and transmit the optical signal by a successive reflection at the upper and lower boundary interface between the core with refractive index n'_1 and a cladding with refractive index n'_2 where $n'_1 > n'_2$ as shown in Figure 2.7 [23].

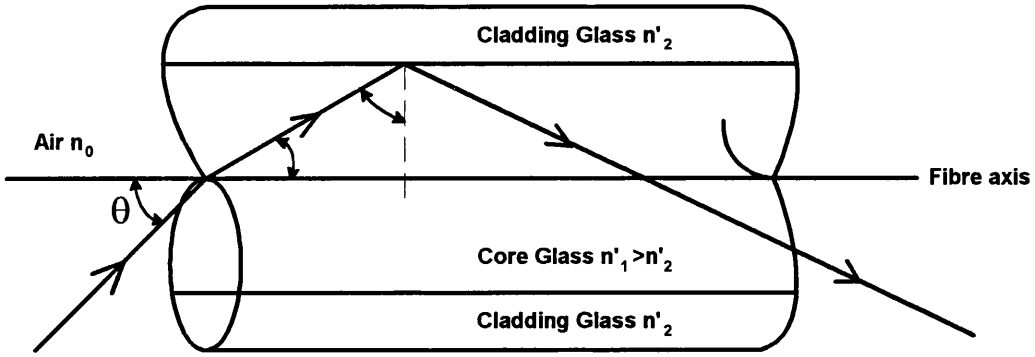

Figure 2.7 - Light Guidance in Optical Wave Guide

In order to launch the light ray into the core of an optical fibre efficiently and to fulfil the condition required of total internal reflection at a core-cladding interface, the ray of light must enter the core at an angle given by:

$$\sin\theta = \sqrt{n_1'^2 - n_2'^2} \qquad (2.3)$$

The greatest possible angle at which the light enters the optical fibre is called the **acceptance angle.** It is only dependent on the two refractive indices n'_1 and n'_2 of the core cladding respectively, and its sine determine the ability of the fibre to accept light and it is called the **numerical aperture** [24].

Based upon the above consideration it might be thought that any ray entering the core of the fibre at an angle less than the maximum acceptance angle will be guided. However, this is not true because, so far, the wave nature of light has been ignored [1]. Hence, in order to obtain an improved model of light propagation in optical fibre the electromagnetic wave theory based upon Maxwell's equation for a medium with zero conductivity must be considered. The interference between the incident and reflected rays requires a constructive interference after two successive reflections at upper and lower boundary interface between core and cladding for such a ray to

propagate indefinitely while still guided. Consequently, there are specific rays (electric field distribution) allowed to propagate in the direction parallel to fibre axis [4]. This electric field distribution is known as a mode and it is only obtained when the propagation vector and the interface have a particular value. In conclusion, light propagates in optical fibre in the form of discrete modes, each of which is specified by a distinct value of θ.

Optical fibre may be classified according to the shape of the refractive index of the core and the number of modes supported. Hence, based on this criteria, three categories of optical fibre emerge, they are: Monomode step index fibre where the core refractive index is constant along and across the core and is slightly greater than that of the cladding, such fibre have a small core diameter, it is widely used in optical fibre sensors based on phase modulation to encode the measurand [2]. Multimode step index fibre and multimode graded index fibres (a refractive index is referred to as graded index when the core index n(r) decreases with radial distance from a maximum value of n_1 at the axes to a constant value n_2 beyond the core radius in the cladding). The number of modes (M) allowed to propagate guided by the fibre is given by $4f_n^2/\pi$, such fibre is also characterised by large core diameter (usually larger than 50μm) [2], where f_n is the normalised frequency.

Multimode fibres are used in optical fibre sensor when high intensity is required because the optical power can be launched into the fibre with reasonable efficiency.

A number of types of specialised optical fibres have been developed recently for use in optical sensing sensors. They differ from the usual fibres by the modified shape of the fibre core, the refractive index distribution along or cross the fibre for instance,

photo-induced effects and the material from which are made. Typical examples of specialised fibres are D-shaped fibre, Hollow-section fibre...

2.3.2 - Dispersion

A pulse of light injected into an optical fibre emerges at the output somewhat elongated due to delay introduced into transit time, a phenomenon known as ***dispersion.*** When a series of pulses are transmitted through a multimode optical fibre, each pulse broadens and may overlap with its neighbours. Eventually some pulses become indistinguishable at the receiver input then errors are more likely to be encountered [19].

The pulse broadening may result from the propagation delay difference between the fastest and the slowest mode since they travel with different velocity. This is known as ***modal dispersion*** and it occurs only in multimode optical fibre. Modal dispersion may be reduced by adoption of an optimum index profile, which is provided by the near parabolic profile of most graded index fibre. Hence, the overall pulse broadening in multimode graded index fibre is far less than that obtained in multimode step index fibre.

The pulse broadening may also result from the propagation delay differences between the spectral components of the transmitted pulse since the optical source may emit a band of frequencies. This is known as ***chromatic dispersion*** and it may occur in all types of optical fibre. The delay differences may arise from the dispersive properties of the waveguide material (***material dispersion***), and also from guidance effects within the fibre structure (***waveguide dispersion***). As can be seen from the diagram below which represents a plot of material dispersion parameter against

wavelength for a pure silica fibre, the magnitude of material dispersion tends to zero in the region of longer wavelengths with absolute zero value at 1.55 μm while it takes the maximum values at the shorter wavelength region as shown in Figure 2.8 [25].

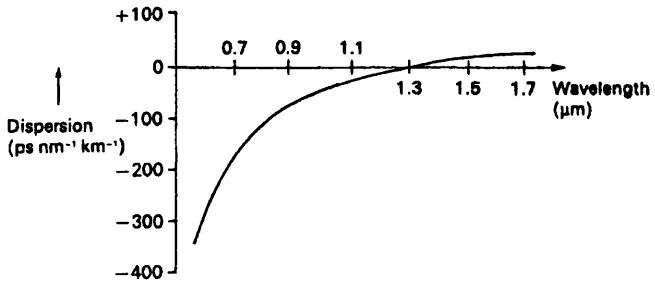

Figure 2. 8 - Dispersion Parameter for Silica as a Function of Wavelength

The negative sign of the dispersion in the region below 1.3 μm indicates that shorter wavelengths travel more slowly than longer wavelengths radiation [1]. Waveguide dispersion is almost absent in multimode fibre but it is significant in single mode fibre. The reduction of dispersion magnitude is important for transmission of high information bit rates in a fibre optic communication system.

The multimode step index fibre exhibits the largest amount of dispersion of transmitted light pulse and multimode graded index fibre demonstrates a considerably enhanced performance. Single mode optical fibre exhibits the minimum pulse broadening and therefore is capable of the greatest transmission bandwidths, which are usually in the Giga hertz range.

2.3.3 – Attenuation

The optical energy propagating in an optical fibre is attenuated. Attenuation is one of the transmission characteristics of most interest to be considered while designing

an optical fibre and is of paramount importance when the suitability of optical fibre for communication purposes is investigated. Then, it should be kept to the minimum level in order to increase the transmission distance without using repeaters. Since the advent of optical fibre with total attenuation of 20 dB/km, measured at μm wavelength [26], this level was viewed as the minimum level acceptable to be reached before an optical fibre can be proposed as an alternative to the coaxial cable as transmission medium. Many works were conducted in research environment to further reduce losses. Typical losses as low as 0.155 dB/km for fused silica and 0.16 dB/km for GeO_2 doped fibre at wavelength of 1.55 μm have been achieved [27]. It has been found that the limit of fibre attenuation is restricted by Raleigh scattering at shorter wavelengths and by vibrational absorption at longer wavelengths [28, 29].

There are several factors responsible for attenuation in optical fibre and they may be categorised within two different categories, namely, intrinsic and extrinsic. The first category include losses related to the design of the fibre and material composition from which it is made for example, light scattering, absorption, leaky mode. The second category includes sources of losses arising from deployment and environmental factors such as bending and mode coupling.

Material absorption arises mainly from the material composition and the fabrication process, which results in generation of heat within the fibre. It is more significant in the ultraviolet and infrared region. Ultraviolet absorption is caused by transition of electrons from the valence band as a result of interaction of photons having a sufficient energy. By contrast the infrared absorption results from the interaction of photons with molecular vibration within the glass. For an absolutely pure silicate glass the absorption is minimal over a wide wavelength band ranging [14] from 0.8 to 1.7 μm, as shown in Figure 2.9.

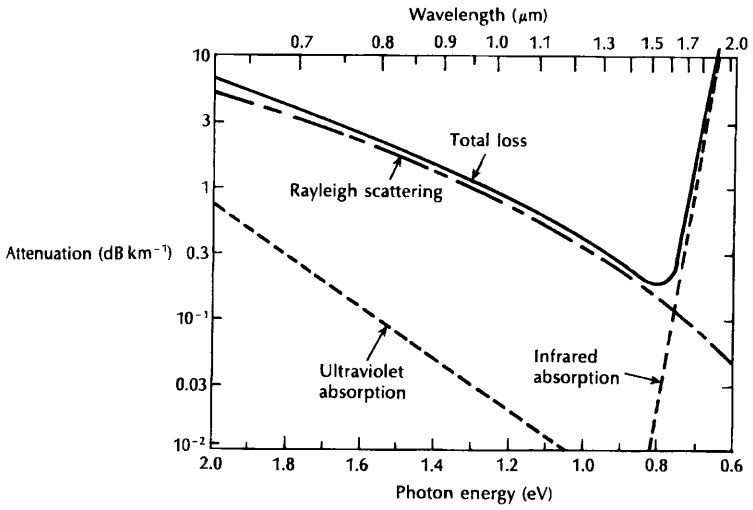

Figure 2. 9 - Attenuation Spectra for the Intrinsic Loss in Pure GeO_2-SiO_2 Glass

Dopants have a great effect on the transmission loss of high silica-glass fibre at long wavelengths. However, by suitable choice of dopant materials such as Germanium, a broad window where losses are below 1 dB/km was obtained in Germanium doped silica with low OH content, the lowest loss level was about 0.46 dB/km at 1.51 μm [30]. Transition metal impurities such as Cu, Ni may contribute considerably to attenuation at long wavelengths. However, their effect may be largely eliminated by a glass refining technique for instance vapour phase oxidation [3]. Another major impurity contributing to absorption in glass is the OH group. Bonded into the glass structure, OH groups have a `fundamental stretching vibrations which give rise to overtones as shown in Figure 2.10. These overtones appear more significantly at about 0.95, 1.24, and 1.38 μm [31, 32, 33].

The last overtone is the strongest absorber [33]. Low-OH-content optical fibres consisting of borosilicate-cladding phosphosilicate-core have been produced by a chemical vapour deposition technique. It results in the disappearance of the second

and the third overtone, thus the first overtone is the only left, but its peak height is considerably reduced [34].

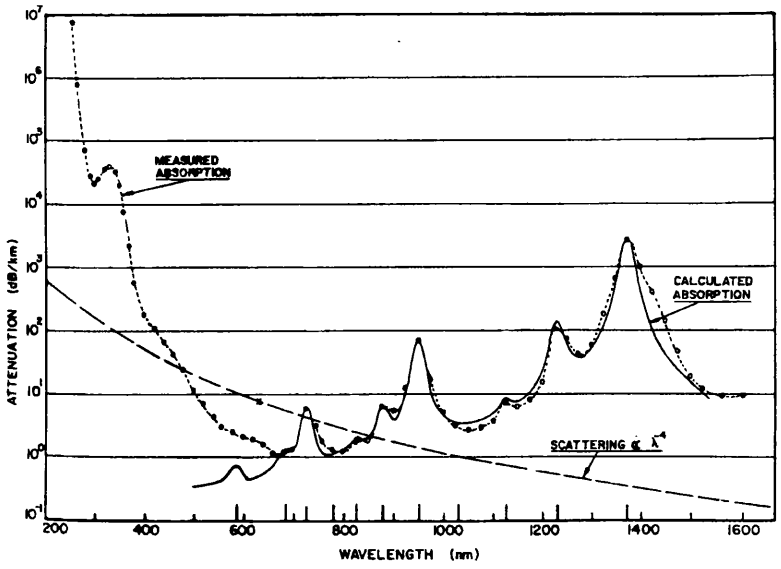

Figure 2.10 - Measured and Calculated Absorptive and Scattering Attenuation as a Function of Wavelength

2.3.3.1 - Linear Scattering of Light

The optical energy contained within one propagating mode may be transferred linearly to the leaky or radiation mode. This linear scattering of light may result from refractive index fluctuation frozen in the glass lattice **(Rayleigh Scattering)** or from the non-perfect cylindrical structure of the fibre optic **(Mie Scattering).** The Raleigh scattering produces an attenuation proportional to $1/\lambda^4$ and the Raleigh scattering coefficient γ_R for a single component glass is given by:

$$\gamma_R = \frac{8\pi^3}{3\lambda^4} n^8 p^2 \beta_c K T_F \qquad (2.4)$$

Where λ is the optical wavelength, n the refractive index of the medium, p is the average photo-elastic coefficient, β_c is the isothermal compressibility at the effective

temperature T_F (temperature at which the glass can reach a state of thermal equilibrium), K is Boltzman constant. The Rayleigh scattering coefficient is related to the transmission loss factor (transmissivity) of the fibre $\wp$ by the following relationship, where L is the length of optical fibre. Is given by:

$$\wp = e^{(-\gamma_R L)} \tag{2.5}$$

Losses due to Rayleigh scattering set the minimum intrinsic losses in the low absorption window between the ultraviolet and infrared absorption tails. Thus, by operating at longer wavelengths the effect of Rayleigh scattering is largely reduced.

It has been found that the sum of the density and composition fluctuation scattering in K_2O-S_iO_2 is less than the scattering (resulting only from density fluctuation) in pure SiO_2, and therefore the attenuation caused by it exhibited a minimum at a concentration of approximately equal to 25 mole % K_2O. For this particular composition the attenuation is approximately equal to 2/3 of that in pure SiO_2 [35]. In contrast the losses related to Mie scattering can be considerably reduced by removing the imperfections that result from the manufacturing process, careful control of fibre extrusion and coating, and the increase of the fibre guidance, which can be achieved through an increase of the refractive index difference.

2.3.3.2 – Non-Linear Scattering of Light

The light propagating down an optical fibre may scatter light in non-linear way; that is, the optical energy of one mode may be transferred either in the forward or backward direction to the same or, another mode at different frequency, thus contributing to attenuation of light transmitted at specific wavelength. It is only

significant where the optical power is above a threshold power level; consequently the operational optical power is limited. There are two important types of non-linear scattering of light. They are **Stimulated Brillouin Scattering (SBS)** and **Stimulated Raman Scattering (SRS).**

Stimulated Raman Scattering results from the interaction of an incident photon (pump photon) with internal vibration (phonon) of the fibreglass material, which results in emission of a scattered photon having a frequency different from that of the incident photon. SRS may occur in both forward and backward direction [36].

The threshold optical power, which must be launched into a single mode optical fibre before SRS may occur, and may be given [37] by:

$$P_R = 5.9 * 10^{-2} d^2 \lambda \alpha_{dB} \qquad (2.6)$$

Where d and λ are the fibre core diameter and the operating wavelength respectively, α_{dB} is the fibre attenuation. This phenomenon was first observed in CS_2 liquid-filled, hollow-core fibre with a pump power less than 5W where a considerable amount of optical power was scattered [38]. For silica-cored fibres, the long interaction length allowed the first observation of SRS at power levels of the order of 75W [39].

Stimulated Brillouin Scattering may be considered as the modulation of light through thermal molecular vibration within the fibre [19]. The incident optical power creates a travelling acoustic wave via the process of electrostriction, and subsequently, scattering the pump light. The pump light may interfere with the scattering light to generate a standing wave, which again stimulates the acoustic wave via electrostriction process [1]. The frequency of the scattered light is maximal in the

backward direction reduced to zero in the forward direction making SBS a purely backward process.

The threshold optical power, which must be launched into a single mode optical fibre before SBS may occur [37], and it is expressed as follows:

$$P_B = 4.4 * 10^{-3} d^2 \lambda^2 \upsilon \alpha_{dB} \qquad (2.7)$$

Where ν is the source bandwidth, and d, λ, α_{dB}, are as previously specified for SRS. A threshold optical power for SBS has been achieved with less than 1W at 535,5 nm in glass optical fibre [40], and as low as 10 mW in single mode fibre [41]. From the above discussion it is apparent that the losses due to non-linear scattering may be avoided by operating at optical power below threshold value. SBS and SRS are almost absent in multimode optical fibre because its large diameter makes the threshold optical power extremely high.

2.3.3.3 - Fibre Bend Loss

Bending radiation can significantly increase the transmission loss [42]. It may result either from large scale bending for instance large curvature **(macrobending)** for mechanical irregularities in the fibre coating or cable such as diametre variation or, alternatively, they may be caused by random lateral forces imposed by external agencies such as clamps (**microbending**). Macrobending causes loss in the manner as illustrated in Figure 2.11.

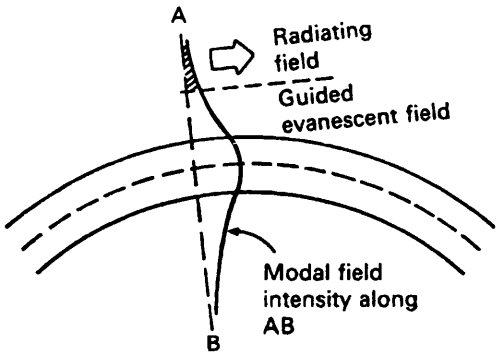

Figure 2.11 - Origin of Bend Induced Attenuation

When a phase front associated with the guided mode penetrates a bend, it must remain plane and perpendicular to the core axis in order for that mode to propagate while still guided. Thus the portion of the energy outside the bend is required to travel faster than that on the inside. Hence, part of the energy in the cladding needs to travel faster than allowed for a wave in that medium. This is not possible, so the portion of energy associated with this part of the mode is lost through radiation. Furthermore, the magnitude of the bend loss can increase dramatically if the curvature radius of the fibre is below a threshold value that can be given by [43]:

$$R_c \approx \frac{3n_1'^2\lambda}{4\pi\left(n_1'^2 - n_2'^2\right)^{\frac{3}{2}}} \qquad (2.8)$$

Here, $n'_1$and n'_2 are core and cladding refractive indices respectively, and λ is the operating wavelength. It is clear from the above expression that macrobending losses may be significantly reduced by designing fibre with large relative refractive index differences, and by operating at the shortest wavelength possible. The magnitude of the loss associated with macrobending [44] may be given by:

$$\alpha_r = c_1 e^{(-c_2 R)} \qquad (2.9)$$

Where R is the radius of curvature of the fibre bend and c_1, c_2 are constants, which are independent of R. This type of loss is also present in single mode fibre and the above criteria for their decrease are also appropriate for single mode fibre design. The amount of power radiated depends on the spot size. If the spot size is reduced, the power is more tightly guided in the core and the pure-bend loss decreases. Bend loss may also arise because coupling between the fundamental mode and the transition modes loses power. In other words, the power distribution in the HE_{11} mode of the straight fibre is different from that of the corresponding mode in the curved fibre, and the power is lost at the interface between the two modes due to this mismatch. This type of bend loss is called ***Transition loss.***

Microbend produces coupling between guided modes and also between these modes and the radiation mode. The amount of the coupled energy becomes more significant when periodic microbends are introduced, if the repeat distance of the bends is related to the difference $\Delta\beta$ between the modal propagation constants or between the propagation constant of guided mode and that of a part of the radiation field.

It is clear from the above discussion that excessive microbending can contribute to an important amount of additional fibre losses. In order to avoid the deterioration of optical fibre transmission characteristics resulting from mode coupling induced microbending, the fibre must be free from any kind of pressure within the cable. In addition a careful controlled coating and cabling should be carried out. This effect can be used to produce sensitive displacement sensors.

For some applications the length of the delivered optical fibre may not be long enough for use in the intended application. So it needs to be jointed to another extension length. Thus, a major consideration with this fibre-fibre connection is the

optical loss encountered in the interface. These losses arise mainly from the three defects of separation, lateral offset and angular misalignment between the ends of two optical fibres [45], they are mainly dependent on the numerical aperture, and are largely independent of the normalised frequency and fibre diameter [46]. In the absence of angular misalignment, the loss is due to lateral offset D only; for a single mode optical fibre it is given by:

$$T_l(\mathrm{dB}) = 2.17\left(\frac{D}{\omega_0}\right)^2 \tag{2.10}$$

Here, ω_0 is the spot size. Whereas the loss due to angular misalignment α only is given by:

$$T_a(\mathrm{dB}) = 2.17\left(\frac{\alpha\omega_0 n_1' f_n}{a\,\mathrm{NA}}\right)^2 \tag{2.11}$$

Here, n'_1 is the core refractive index, NA numerical aperture, f_n normalised frequency of the fundamental mode, and a is the core diameter.

However, if the two jointed ends are smooth and perpendicular to the fibre axes, and the two fibre axes are perfectly aligned, the losses are reduced only to loss due to Fresnel reflection, since a small fraction of light may be reflected back to the transmitting fibre [14], and it may be given by:

$$Loss_{fres} = -10\log_{10}(1-2r) \tag{2.12}$$

Where r is the fraction of light reflected at a single interface. The magnitude of Fresnel loss may be substantially eliminated through the use of an index matching fluid with a refractive index similar to that of the fibre core.

There are two major categories of fibre joint commonly in use. Fibre splices, which are a permanent joint, are widely used in fibre optic telecommunication systems. This type of joint can be formed either by fusion method or mechanical clamping. Heating the interface between two butted, pre-aligned fibres to their melting point, in order to produce a seamless joint, carries out fusion splicing. Mechanical splicing employs an elastomeric tube, in which the ends of the fibre are held in alignment. In addition to these methods just mentioned above, another method of joint that involves the use of glue exists. Being fed into a high precision guide butts the fibres, then they are surrounded by a liquid adhesive, which is finally cured using a portable ultraviolet light. All these splicing techniques require a good quality end faces to be prepared initially.

Fibre connectors, which are a demountable joint, allow a reproducible accurate alignment of the optical fibres, in order to permit connection and disconnection without affecting the performance of the transmission line at the joint. Fibre connectors may be put into two broad categories, which are available for use. These are butt jointed connectors and expanded beam connectors. In butt-jointed connectors the two carefully prepared fibre ends are brought into a close proximity so that the fibre core axes will be in contact with each other. Expanded beam connectors involve the use of lenses to collect and collimate the light emerging from a transmitting fibre end and to focus the beam into the adjoining fibre.

This method provides a better lateral alignment than a butt-jointed fibre connector. Moreover, an acceptable longitudinal separation can be achieved, but this can only be realised at the expense of more stringent angular alignment.

All type of splices is provided to couple all the light propagating in one optical fibre into the adjoining fibre. By contrast an optical fibre coupler is a device that

splits all the light contained into a main fibre into two or more fibres or, alternatively, couple a proportion of the light propagating in the main fibre into a branch fibre. Moreover, these coupler devices are bi-directional i.e. the light from one or more branch fibres can be combined into a main fibre.

2.4 – Optical Detector

The optical output of an optical sensing system must be first converted to the electrical signal, either current or voltage, in order to be processed, then displayed or recorded. To accomplish this task a photodetector is used. Photodetectors may be classified as either thermal or photon. The thermal detector relies upon the transduction of the incident optical energy to heat within the detector, which modulates an electrical current. Since only the total energy is important, the responsivity of the detector is effectively wavelength independent. Whereas the photon detector relies upon the generation of photon carriers as a result of absorption of energy from a single photon that has energy greater than the band gap. In this case it is the energy of a single photon, which is relevant, consequently, the responsivity of the detector is wavelength dependent [1].

The photodiode is the most widely used device to detect the optical energy in optical fibre sensors; a p-n junction basically forms it.

When a photon having an energy (hv) exceeding the band gap E_g is incident upon the photodiode, it is absorbed by the electrons, which make transition to the conduction band leaving behind them unoccupied energy levels or holes in the valence band. This process is known as **photo-generation** of electron-hole (carriers) pairs, it takes place all through the device.

However, in order, to optimise the response of the photodiode, absorption of photon and carriers generation must be maximised in the depletion region [5]. This can be achieved by introducing an intrinsic or lightly n doped material between two heavily doped region p^+ and n^+. This device is called a Pin photodiode. Under the influence of suitable reverse bias the depletion region may extend through the entire intrinsic region as shown in Figure 2.12.

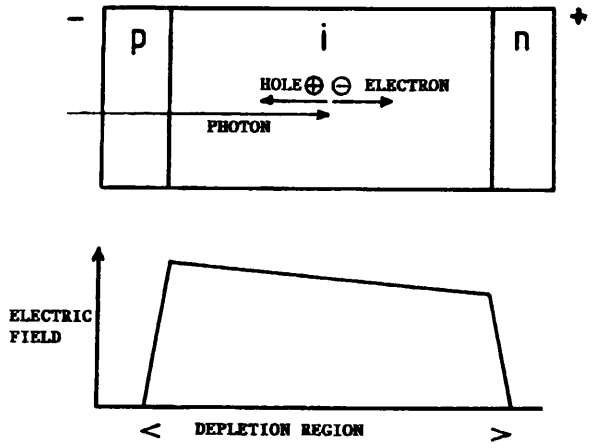

Figure 2.12 - Schematic Diagram of a Pin Photodiode Showing the Electrical Field Distribution of Depleted Region

Another type of photodiode is the so-called avalanche photodiode (APD). Such device include a region of high electric field which accelerate the primary generated photocarriers so that collisions with atoms result in further generation of photon carrier by impact ionisation. These secondary generated carriers can be accelerated by the electric field, thus contributing to further carrier generation; this phenomenon is known as the **avalanche effect.**

A photodiode can operate in two different modes, the photovoltaic mode and the Photoconductive mode. The photovoltaic mode sometimes is also referred to as unbiased mode. The principle of detection relies upon the measurement of voltage

developed across a load resistor as a result of flows of photo-generated carriers in the opposite direction.

On the other hand, the photoconductive mode is sometimes also referred to as the biased mode. The photodiode is reverse biased; an electric current flowing in the external circuit is detected. This current results from the photo-generated carriers separated by the electric field.

2.4.1 - Resolution and Noise

Resolution is an important characteristic of any sensing system; it describes the smallest change in measurand that can be sensed, and it is governed by the noise randomly introduced. Noise may be defined as the random fluctuation of current and voltage in an electrical circuit from physical processes, which are statistical in nature. Noise is characterised by its frequency spectrum, and it may arise from random electron motion due to their 3kT/2 thermal energy (k is Boltzman constant and T is temperature), this type of noise is referred to as **Johnson** noise and it is independent of the frequency, it may also be due to **shot** noise which may result for example from the dark current and photocurrent. Another contribution to the noise is the so-called **flicker** noise; this noise is inversely proportional of the frequency (1/f) and is more pronounced in silicon than germanium devices.

2.5 - Natural Light

Light waves are electromagnetic in nature, thus they require both electric and magnetic fields for their complete description. The electric field E is always chosen to

define the state of polarisation of light for it exerts a much stronger force than the magnetic field does on the electron when light interacts with matter [47]. The state of polarisation may be defined as the curve generated by the end of the electric field vector; for example, if the vibration of the electric vector always lies in the same plane, then the light is termed *plane-polarised.* If it were possible to see the electric vector then on looking at the incoming beam the vector would be seen to be oscillating along a fixed line.

An ordinary light source consists of a very large number of randomly oriented atomic emitters. Thermal or electric discharge excitation of these atoms result in emission of radiation that lasts roughly 10^{-8}s [32]. Waves emitted that have the same frequency will combine to produce a resultant wave having a state of polarisation that changes in an unpredictable fashion. If these changes take place at so rapid a rate as to render any single resultant polarisation state indiscernible, the wave is referred to as *natural light.* It is also known as unpolarised light, but in reality the light is composed of a rapidly varying succession of the different states of polarisation.

The unpolarised light may be represented mathematically in term of two arbitrary, incoherent, orthogonal, linearly polarised waves [49]:

$$\begin{aligned} E_x(t) &= iE_{ox}\cos(\omega t + \varepsilon) \\ E_y(t) &= jE_{0Y}\cos(\omega t) \end{aligned} \tag{2.13}$$

Where ω is the angular frequency, t the time, and ε is the phase difference between E_{0x} and E_{0y}, which are the maximum amplitudes of each component. The resulting optical disturbance may be given by:

$$\begin{aligned} E(t) &= E_x(t) + E_y(t) \\ E(t) &= iE_{0x}\cos(\omega_t + \varepsilon) + jE_{0y}\cos(\omega t) \end{aligned} \tag{2.14}$$

The variation of E_{ox} and E_{0y} and ε defines all polarisation states. For example, setting $\varepsilon=2\pi$ then the two components are in phase and the resultant polarisation is linear i.e.:

$$\begin{aligned} E(t) &= iE_{0x}\cos(\omega t + 2\pi) + jE_{0Y}\cos(\omega t) \\ E(t) &= \cos(\omega t)(iE_{0x} + jE_{0y}) \end{aligned} \tag{2.15}$$

Where the term ($iE_{0X} + jE_{0y}$) is the fixed amplitude of the resultant disturbance. Conversely setting $\varepsilon=\pm\pi$ the two waves will be out of phase by 180° then the optical disturbance is given by:

$$E(t) = \cos(\omega t)(-iE_{0x} + jE_{0Y}) \tag{2.16}$$

Which is again a linearly polarised wave but the plane of vibration has been rotated by 90° (if $E_{0x} = E_{0y}$).

Extending this analysis further, $E_{ox} = E_{oy} = E_0$ and if E_x (fast axis) leads E_Y (slow axis) by ($\varepsilon=\pi/2$) then the resultant disturbance becomes:

$$\begin{aligned} E(t) &= iE_0\cos\left(\omega t + \frac{\pi}{2}\right) + jE_0\cos(\omega t) \\ E(t) &= E_0\left[-i\sin(\omega t) + j\cos(\omega t)\right] \end{aligned} \tag{2.17}$$

The scalar amplitude is constant but the direction of E is time varying. For this particular disturbance then at t=0.

$$E(t) = jE_0 \tag{2.18}$$

And at later time $t = t_0$, then:

$$E(t) = E_0\left(-i\sin(\omega t_0) + jE_0\cos(\omega t_0)\right) \tag{2.19}$$

Plotting these results on a Cartesian graph for t= 0, E(t) defines a reference axis along the y axis, Figure 2.13. At the later time t_0, E(t) shifts *anti clockwise* to lie along the axis as shown.

From Figure 2.13 the resultant electric vector is rotating anti-clockwise with angular frequency ω for an observer towards whom the light is seen. This optical disturbance is said *left handed circularly polarisation.*

Alternatively if E_x (slow axis) lags E_y (fast axis) by $\pi/2$ ($\varepsilon=-\pi/2$) the resultant optical disturbance will be *right handed circularity polarised.* The Figure 2.14 shows a variety of polarisation states for different values of ε and E_{0x} and E_{0y}.

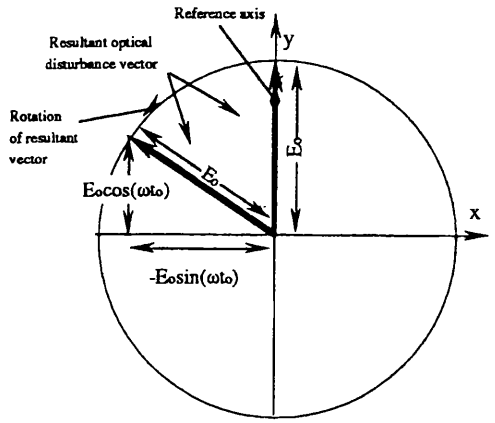

Figure 2.13 - Left Handed Circularly Polarised Light

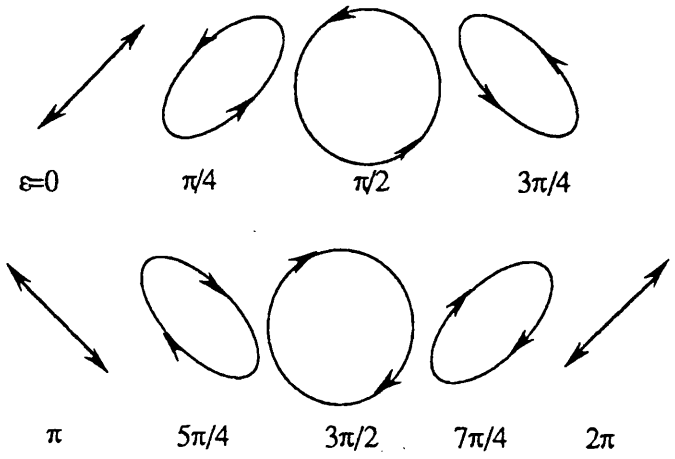

Figure 2.14 - Polarisation States Corresponding to Specific Values of ε.

2.6 - Polariser

An optical device whose input is natural light and whose output is some form of polarised light is known as a *polariser.* For example, an instrument, which separates the two orthogonal components of unpolarised light, discarding one and passing on the other, is known as a ***linear polariser***. Polarisers take on many different configurations, but they are all based on one of four fundamental physical mechanisms: dichroism or selective absorption, reflection, scattering and birefringence or double refraction.

In the very broadest sense the term dichroism means selective absorption of one of the two rectangular components comprising an ordinary incident beam and transmission of the other component. The earliest usage applied to naturally occurring dichroic crystal such as tourmaline [50]. When a beam of light is made to pass by a tourmaline, it emerges polarised. This is due to a selective absorption by the tourmaline of light rays vibrating in a plane perpendicular to the optic axis while the component vibrating in a plane perpendicular to the optic axis at right angle to the previous one is not affected [51]. This can be easily verified by using another tourmaline.

With the two tourmalines set parallel to each other, the second one also transmits the light transmitted by the first crystal. While, when 90 rotate the second tourmaline, i.e. the two tourmalines are set crossed, as shown in Figure 2.15, of light occurs [52, 53].

The most important use of dichroism is in man-made dichroic devices, the simplest of which is the wire grid polariser which polarises natural light linearly by absorbing the electric field component parallel to the wire and transmission of the component

perpendicular to it, provided that the wavelength of the incident light is much smaller than the spacing of the wire grid [32] as shown in Figure 2.16.

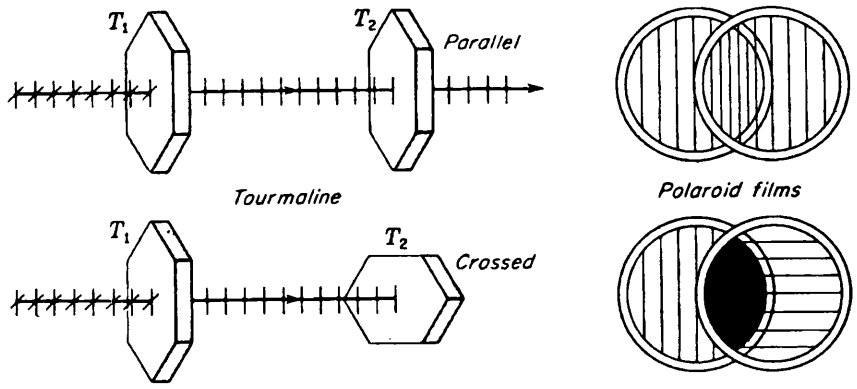

Figure 2.15 – Parallel and Cross Tourmaline Grid Junction

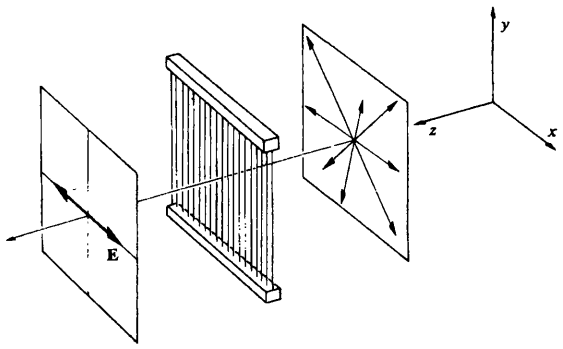

Figure 2.16 - A Wire Grid Polariser

The component of light parallel to the wires sets the free electron in a forced oscillatory motion. This oscillating electron constitutes a dipole, which radiates the electromagnetic energy in all directions except the direction of vibration itself [54].

Evidently, the superposition of an incident electromagnetic wave with vertical E-vibrations and the radiation of these electron oscillators lead to cancellation in the forward direction, through destructive interference. In addition, the oscillation of the

free electrons is not entirely free. The effective friction due to interaction with lattice imperfections, for example, constitutes some dissipation of energy, which must attenuate the incident wave. In contrast, the electrons are not free to move in the horizontal direction therefore the incident electric field is unaltered as it propagates through the grid. The transmission axis of the grid is perpendicular to the wires.

The first man-made dichroic based on this principal was the dichroic sheet polariser known commercially as Polaroid *J-sheet*, invented by Herapath. A colloidal suspension of the herapathite needles was extruded between long narrow slits. As the sheet was extruded, the needles were oriented parallel to one another [55]. The scattering of light because of submicroscopic size of the crystals constitutes a major drawback of using such a polariser.

Ten years later Land invented the H-sheet polariser, which is now probably the most widely used linear polariser. This type of polariser consists of a long molecular chain of polyvinyl alcohol heated and stretched in a given direction so that its long molecules line up in the direction of stretching. Then, the sheet is immersed into an ink solution rich in iodine. The iodine impregnates the plastic and becomes associated with the linear molecules, providing conduction electrons, which can move freely along the chains as if they were long thin wire. *HN-50* would be the designation of a hypothetical, ideal *H*-sheet having a neutral colour (N) and transmitting 50 % of the incident natural light while absorbing the other 50 %, which is the undesired polarisation component.

2.6.1 - Polarisation by Birefringence or Double Refraction

When an electromagnetic wave is incident on a dielectric, it will excite the electron-oscillators and drive them into a forced vibration, which results in radiation or scattering of energy in the form of electromagnetic wavelets.

In a material whose atoms or molecules are arranged with some degree of regularity (isotropic medium), the secondary and primary wavelets recombine to form only one refracted wave. The resultant or refracted wave will lag the incident (free space) wave by some amount if the frequency of the incident electric field is below resonance i.e. the natural frequency of the electron-oscillators. In contrast, above resonance the refracted wave will lead the incident wave. The index of refraction for a material with N molecules per unit volume, each with f_j oscillators having natural frequencies ω_{0j} may be expressed by the so-called ***dispersion equation***.

$$n^2(\omega) = 1 + \frac{Nq_e^2}{\varepsilon_0 m_e} \sum_j \left(\frac{f_j}{\omega_{0j}^2 - \omega^2} \right) \qquad (2.20)$$

Where m_e and q_e are the mass and charge of electrons respectively. The above equation is an over-simplification of the phenomenon known as dispersion, and an additional damping term should have been included in the denominator of the sum. This damping term arises, in part, from energy lost when the forced oscillators in turn reradiate the electromagnetic energy, and in other part from the dissipation of energy in the form of heat resulting from the strong atoms and molecule mutual interaction. This latter process is called ***absorption.*** As ω increases towards ω_{0j} then $(\omega_{0j} - \omega)$ decreases and $n(\omega)$ gradually increases with frequency. This is called ***normal dispersion.*** A further increase of ω towards ω_{0j} has, as consequence, the resonance

of the oscillators, and their amplitude will increase considerably and this will be accompanied by damping and strong absorption of energy from the incident wave. The damping term becomes dominant when ($\omega_{0j}=\omega$), and the frequency interval surrounding ω_{0j} is called ***absorption band.*** In such an interval $(dn/d\omega)$ is less than zero and the process is referred to as ***anomalous dispersion*** as shown in Figure 2.17.

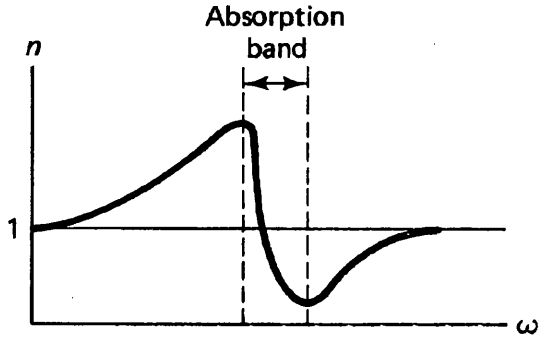

Figure 2. 17 - Response of Refractive Index as a Function of Frequency Near the Absorption Band

However, there are many crystalline materials that present certain symmetric irregularities in atoms distribution which result in anisotropy in the binding force. Such crystals are said to be **anisotropic** (i.e. their optical properties are not the same in all directions), the dichroic crystals mentioned previously are a special subgroup. The mechanical model of an anisotropic material can therefore be represented by a charged shell (electrons) bound by springs having different stiffnesses to a fixed point (nucleus), Figure 2.18.

The electron will have a natural frequency ω_0 proportional to the square root of the spring constant. If now we consider the incidence of light upon such an isotropic material, the speed of the refracted wave, and therefore the index of refraction, will be determined by the difference between the frequency of the E-field and the natural or characteristic frequency of the electron-oscillators. For example, if the electric

field is parallel to the stiff springs, i.e. in a direction of strong binding force along the x-axis, the electron's natural frequency would be high (proportional to the square root of the springs constant). In contrast, if E is along the y-axis where the binding force is weaker, the natural frequency would be somewhat lower. An anisotropy in the binding force will therefore be manifested in an anisotropy in the refractive index, which may have a form similar to that given by Figure 2.19.

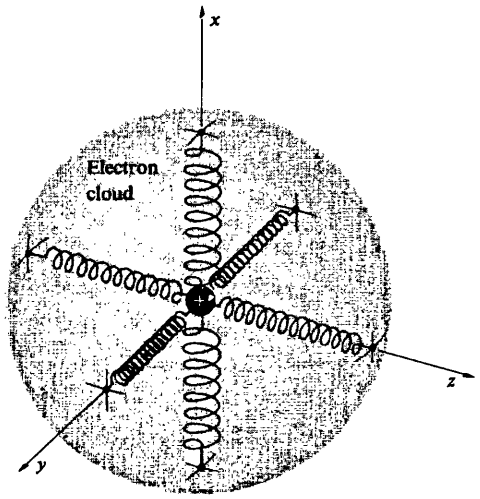

Figure 2.18 - Mechanical Model of an Anisotropic Material

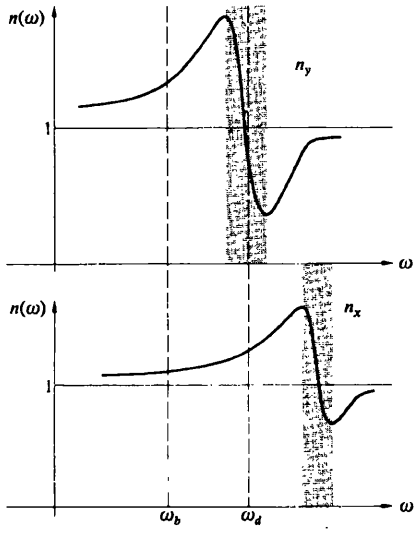

Figure 2. 19 - Refractive Indexes Versus Frequency Along Two Axes in a Crystal

Regions where $dn/d\omega < 0$ is said to be a region of anomalous dispersion. A material which displays two different refractive indices is said **Birefringent.** If the frequency of the incident light resides in the vicinity of ω_d that is in the absorption band of the $n(\omega)$, the crystal will be strongly absorbing for the polarisation components in (y) direction, whilst the other components will transmitted unaffected.

A crystal, which is transparent to one polarisation component and absorbing to the other component, is in fact ***dichroic***. Further, if the crystal is such that the binding forces in y and z directions are equal, the x-axis then defines the optic axis.

However, more often, the natural frequencies of a birefringent crystal are above the optical range, i.e. the incident wave is considered to have frequencies in the region of ω_b where the absorption for either polarisation components is negligible and the crystal has two different refractive indices. Consider a ray of light incident normally upon a birefringent crystal such as calcite having the above characteristic at frequency residing in ω_b region. On entering the crystal it splits up into two plane polarised rays at right angles to each other, namely: the ordinary ray which lies in the same plane as the incident ray and, therefore, obeys the ordinary refraction law in an isotropic medium, that is the direct prolongation of the incident ray, and the extraordinary ray which lies in the plane perpendicular to the ordinary ray and follows a law of refraction different from that of an isotropic mediums [56], Figure 2.20.

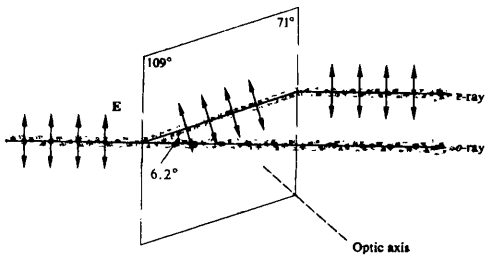

Figure 2.20 - A light Beam with Two Orthogonal Field Components Traversing a Calcite Principal Section

This phenomenon is known as double refraction or **Birefringence.** It was first discovered in 1669 by Bartholinus who observed two images when he looked at an object through a crystal of Iceland spar [57]. Since the refractive indices of a plate for the ordinary and extraordinary rays differ, it follows that the two rays traverse the plate with different velocities and, therefore, emerge from the plate out of phase.

There is, however, a special direction in which both of the waves have the same propagation velocity and the two waves are superimposed. This particular direction is called the **optical axis**, and if the crystal has only one optic axis the crystal is said to be **uniaxial.** If there are two directions in which the anisotropy is not verified, i.e. the crystal behaves as an isotropic material, the crystal is said to be **biaxial.** In addition, the crystal is said to be negative or positive material according to whether the ordinary wave leads or lags the extraordinary wave respectively. The axis along which the retarded component is propagating is called the slow axis while the other axis i.e. along which the fast component propagates is called the fast axis.

If a relative phase difference of $\Delta\varepsilon = \pi/2$, which is also sometimes referred to as retardation, is introduced between the two polarisation components i.e. the ordinary and the extraordinary waves the plate is termed a q*uarter-wave* plate because a phase difference of 90° corresponds to a path difference of λ/4, where λ is the wavelength of the incident monochromatic light. Quarter-wave plates are often used to convert an elliptical polarisation to a linear one and vice versa. In addition, when linearly polarised light falls at an angle of 45° to either principal axis of a quarter-wave plate, the ordinary and extraordinary rays will have the same amplitude. Under this condition a phase shift of 90° converts a linearly polarised light to the circular one. In the same way, an incoming circular polarised light will be converted to the linear one.

Similarly, if a relative phase difference of π radians or 180° is introduced between the ordinary and extraordinary waves, the retarding plate is said to be a *half wave-plate*. If an incident beam makes an arbitrary angle σ with the fast axis of a negative crystal, the extraordinary wave will propagate through the plate faster than the ordinary wave with a longer wavelength. Hence, the introduced relative retardation increases as the waves progresses through the plate, therefore the state of polarisation gradually changes from one point to another. On emerging, the two waves will experience a phase shift of $\lambda/2$, and the electric field vector will rotate through 2σ. In conclusion, the half-wave plate can be used to invert the handedness of circular or elliptical light, changing right circularly polarised light to left-circularly polarised light, or vice-versa and can be also used to change the right-elliptically polarised light into left-elliptically polarised light and at the same time "reflect" the major axis of the ellipse [48].

Commercially the wave plates are generally specified by their relative linear retardation, which might be, for example, 140 nm for a quarter-wave plate. The retardation of a wave-plate can be modified from its designated value by tilting it somewhat. For example, if the wave plate is relatively rotated about the fast axis, the retardation increases while a rotation about the slow axis causes the retardation to decrease.

Light can also be polarised more or less completely by reflection, at an appropriate angle, from the surface of a transparent medium. When unpolarised light falls upon a dielectric such as glass, there will always be a reflected ray and a refracted ray. Experiments shown that the reflected ray is partially plane-polarised Brewster discovered that light is almost completely polarised in the plane of incidence when

reflected from a transparent medium at a particular angle, termed Brewster angle or polarisation angle, this angle differs from one medium to another [58, 59].

The removal of energy from an incident wave by some scattering medium and the remission of some portion of the energy in many directions are known as **scattering** [48]. The polarisation of light by scattering has no advantages over other methods in laboratory practice but it has a great importance as a natural phenomenon. If a plane-polarised light is made to fall upon an air molecule, the interaction yields a scattered plane-polarised light in all directions except in the direction parallel to that of atomic vibration in which no light is emitted. Whereas if the incident light is un-polarised the scattered light in the forward direction is completely un-polarised; off that axis it is partially polarised, becoming increasingly more polarised as the angle increases. When the direction of observation is normal to the primary beam, the light is completely linearly polarised.

2.7 - Conclusion

To sum up, two different classes of optical fibre sensors are currently in use namely, intrinsic and extrinsic. To energise these sensor devices a wide range of optical sources exists, the choice of a suitable source is determined by the type the optical fibre used. For sensors based upon multimode fibre coherent sources such as LEDs and Halogen-Tungsten sources are usually used. Whereas for sensor based upon monomode fibre a coherent source such as laser is appropriate. The nature of signal processing also has a big influence on choosing a suitable source.

The optical signal transmitted by an optical fibre suffers from attenuation or losses. The reduction of losses has great importance, and it is of most importance where the

intensity is modulated as a function of the measurand. With this variety of optical fibre sensor, optical sources and the variety of propagation constant properties of optical signal, different types of detection techniques can be profitably exploited. However, the most widely device used to detect the optical signal is the photodiode.

CHAPITRE 3

OPTICAL STRAIN GAUGE DESIGN

3.1 - Introduction

A variety of optical fibre techniques have been developed for strain measurement. In particular this project investigates an optical fibre sensing system based upon small variable birefringent elements for pantograph of high-speed railroad vehicles application. The modulation of the optical signal consists of producing spectral changes by passing a polychromatic light through a photo-elastic material subjected to the force to be measured.

The returned chromatic signal is detected using a double layer photodiodes each having different but overlapping wavelength sensitivities. The ratio of the output from the two layers varies with spectral signature of the received optical signal. This chromatic sensing technique is preferred, because it enables intensity insensitive measurement to be made. In addition, the optical technique provides complete electrical isolation from the 25 kV lines. In this project, an optical strain measuring system as described above is to be used as the sensing element in a closed loop control for power collectors for electric trains.

3.2 - Stress Induced Birefringence

Many optically isotropic transparent materials can become anisotropic when subjected to an applied stress or induced strain through an elasto-optic interaction

known as **stress birefringence**, or the **photo-elastic effect**, and therefore display optical characteristics similar to those of a birefringent crystal [60].

The applied stress acts in a way to change the inter-atomic structure of the body, which alters its optically isotropic character. This effect persists while loads are maintained but vanishes, almost instantaneously or after some interval of time when the loads are removed, hence the qualified term of "temporary birefringence" [61]. The discovery of the temporary birefringence or the double refraction under strain was made in 1816 by David Brewster and marked the beginning of the science of photo-elasticity [62, 63, 64].

As is well known, when a body is subjected to a three dimensional stress system, there exist at each point of the body three mutually perpendicular planes across which the resultant stress is normal [65]. These planes are called the principal planes of stress and correspond, in material exhibiting a temporary double refraction, to the principal sections of the crystal represented by an element of the material at that point. The directions of these normal stresses correspond to the principal crystallographic axis [66]. There is thus, a direct relationship between the ellipsoid of stress and the index ellipsoid. At any point of the material under an orthogonal three-dimensional stress (σ_1, σ_2, σ_3), the optical properties can be represented by an index ellipsoid, the principal axes of which coincide with the principal axes of stress at the point. Based upon the co-axciality of Fresnel's index ellipsoid and Cauchy's stress ellipsoid, Maxwell in 1852 expressed the relationships between the principal refractive indices and the principal stress [65]:

$$n_1 - n_2 = c(\sigma_1 - \sigma_2) \tag{3.1}$$

$$n_1 - n_3 = c(\sigma_1 - \sigma_3) \tag{3.2}$$

$$n_2 - n_3 = c(\sigma_2 - \sigma_3) \tag{3.3}$$

Where c is known as the stress optic coefficient. n_1, n_2, and n_3 are the principal refractive indices for waves vibrating parallel to the principal stresses σ_1, σ_2, σ_3 respectively.

Similarly, the state of strain of a three-dimensional body can be represented by a symmetric strain tensor at each point of the body considered. For an elastically deformed body, both the stress and strain tensors have the same principal directions; therefore, their respective stress and strain ellipsoids, or the so-called Cauchy ellipsoids, are coaxial [65]. Thus using Hook's stress-strain relationship between the principal refractive indices and the principal strain the following relationships emerge:

$$n_1 - n_2 = k(\varepsilon_1 - \varepsilon_2) \tag{3.4}$$

$$n_1 - n_3 = k(\varepsilon_1 - \varepsilon_3) \tag{3.5}$$

$$n_2 - n_3 = k(\varepsilon_2 - \varepsilon_3) \tag{3.6}$$

Where n_1, n_2, n_3 are as specified previously, k is called the strain optic coefficient, and ε_1, ε_2, ε_3 are the principal strains. A plane polarised light wave vibrating in a plane containing the axis of principal stress, of the ellipsoid, emerges from the material unchanged except for a loss of intensity. For any other direction of vibration with normal incidence, the wave is resolved into two components vibrating in two mutually perpendicular planes AOC and BOC respectively, Figure 3.1.

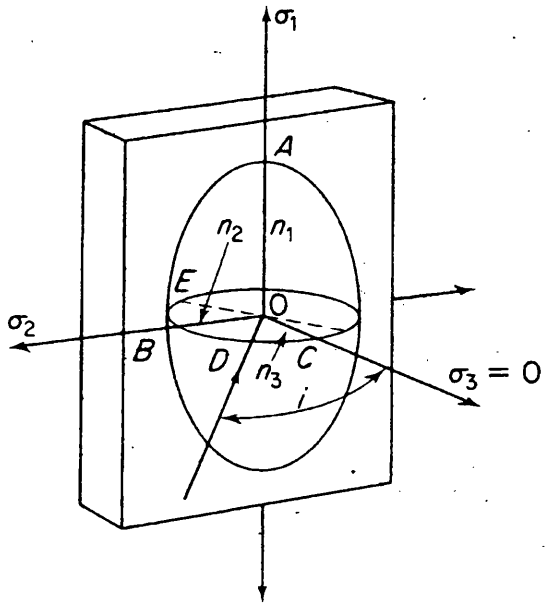

Figure 3.1- Index Ellipsoid for a Point in a Uniaxial Stress Field

Moreover, since the stress coefficients are unequal, it follows that the refractive indices in both these planes will be different consequently these two components will travel with different velocities. Thus, on emerging from the photo-elastic medium, the two components will have suffered a relative change of phase or relative retardation (δ) that is proportional to $(\sigma_A - \sigma_B)$ [67] (Figure 3.1), and it can be given by:

$$\delta = (n_1 - n_2)\chi = c\chi(\sigma_A - \sigma_B) \qquad (3.7)$$

Where c is the stress optic coefficient, χ is the thickness of the photo-elastic material, σ_A, σ_B are the stress coefficients along OA and OB respectively. n_1, n_2 are the refractive indices along OA, OB respectively.

In the case of uniaxial stress (strain) for example the stress coefficient along OB equal to zero (σ_B=0) the relative retardation will be given by:

$$\delta = (n_1 - n_2)\chi = c\chi\sigma_A \qquad (3.8)$$

Where χ is the thickness, n_1, n_2, c, σ_A are as specified previously. That is, the polarisation component oscillating parallel to OA would lag the component orthogonal to this direction by δ for a propagation distance χ.

3.3 – Photo-elasticity

Photo-elasticity is a powerful and accurate experimental technique for stress and strain analysis; it can be applied under two circumstances [68].

The first circumstance occurs with an already existing structure. In such structure the photo-elasticity can be used to provide qualitative information about the general distribution of stress, position of stress concentration and areas of low stress produced during some mechanical deformation. These results can be exploited to modify the design in order to reduce or disperse the concentrations of stress, thereby achieving reduction in weight and material cost [61].

The second circumstance occurs during the design process itself where stress conditions are evaluated and taken into account before production so that the failures of the component during production, the necessity of design modification and re-tooling, may thus be avoided. In addition, photo-elastic analysis provides an effective method of failure investigation, hence producing valuable information leading to successful re-design. The name photoelasticity reflects the nature of this experimental technique: *Photo* implies the use of light rays and optical techniques, while *elasticity* depicts the study of stresses and deformations in elastic bodies [69].

This analysis is carried out through an optical instrument known as **polariscope** that utilises the properties of polarised light. Two types of polariscope are commonly employed in stress analysis work, the **plane polariscope**, and the **circular**

polariscope. the plane polariscope is the simplest optical system used in photo-elasticity; it consists of two linear polarisers (which transmit light only along their axis of polarisation) and a light source. The linear polariser nearest the light source is called the *polarizer*, while the second linear polariser is known as the *analyser*. In the plane polariscope, the two axes of polarisation are always crossed; hence no light is transmitted through the analyser.

The circular polariscope employs circularly polarised light. Quarter-wave plates (i.e. $\lambda\backslash 4$ plates) are introduced between the polariser and the plate, and between the plate and the analyser. The material of the quarter-wave plate is initially bi-refringent; they have been introduced to eliminate the isoclinic fringe from the field of view without modifying the isochromatic fringes; this considerably facilitates isochromatic fringe reading [69].

3.4 - Application of Stress Birefringence to Chromatic Modulation

Consider a linearly polarised light produced by selective absorption incident normally upon a transparent plastic of thickness χ, placed in a plane polariscope, subject to bi-directional stress along the principal direction A and B (Figure 3.2).

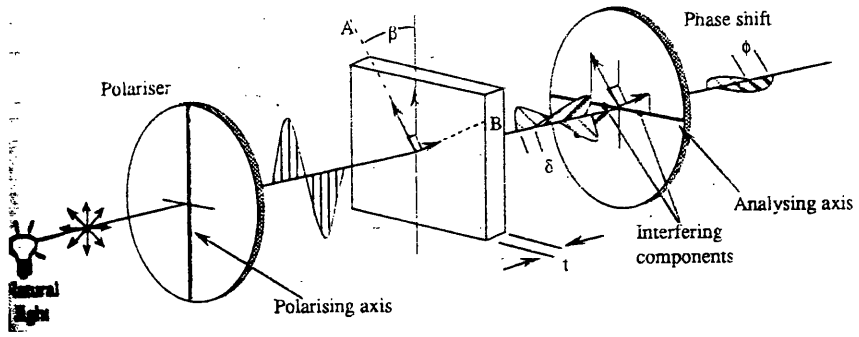

Figure 3.2 - Polarised Light Propagating Through Stressed Plastics [70]

On entering the plate, the light vector will be resolved into two orthogonal components which propagate with different velocities in the planes A and B and emerge from the plate out of phase.

Note that the stress and strain intensities induced along A and B, are σ_A, σ_B and ε_A, ε_B respectively. It follows from the precedent equation which established that the relative change in index of refraction is proportional to the difference between these strains and stress, it can be found that the relative retardation developed between the two waves is given by:

$$\delta = (n_A - n_B)\chi = c(\sigma_A - \sigma_B)\chi = k(\varepsilon_A - \varepsilon_B)\chi \qquad (3.7)$$

Where k is Coefficient of optical sensitivity to strain. These equations may be reduced in the case of uniaxial stress for example ε_B equal to zero.

$$\delta = (n_A - n_B)\chi = c(\sigma_A)\chi = k(\varepsilon_A)\chi \qquad (3.8)$$

That is the polarisation component parallel to A i.e. in the same direction as the strain lags the components parallel to B by δ under tensile stress/ strain for propagation distance χ [70]. By inserting a second linear polariser (analyser) with its transmission axis perpendicular to that of the polariser, only the components horizontal will be transmitted and combined to produce interference fringes. It can be shown that the intensity of light emerging through the second polariser i.e. the analyser [66] is given by:

$$I = I_\lambda \sin^2(2\beta)\sin^2\left(\frac{\pi\delta}{\lambda}\right) \qquad (3.9)$$

If light is monochromatic.

$$I = \sum_{\lambda} I_{\lambda} \sin^2(2\beta)\sin^2\left(\frac{\pi\delta}{\lambda}\right) \tag{3.10}$$

If light is polychromatic.

If the analyser and polariser axis are set parallel to each other, it follows that the intensity transmitted is given by:

$$I = I_{\lambda}\left(1 - \sin^2(2\beta)\sin^2\left\{\frac{\pi\delta}{\lambda}\right\}\right) \tag{3.11}$$

And,
$$I = \sum_{\lambda} I_{\lambda}\left(1 - \sin^2(2\beta)\sin^2\left\{\frac{\pi\delta}{\lambda}\right\}\right) \tag{3.12}$$

for monochromatic and broadband sources respectively.

It is clear from the above equations that there are two conditions under which extinction of light may take place. The first condition is when the principal stress direction β is at 0 or $\pi/2$ with respect to the polariser / analyser axis. The intensity transmitted will be zero, whatever the wavelength and whatever the magnitude of σ_A, σ_B.. Thus a black fringe called an isoclinic is observed that provides the locus of those points in the structure at which the principal stresses have a given direction (that of the polariser and analyser axes). Hence, by rotating the polarizer and analyser, still with their transmission axis crossed relatively to the plate until an isoclinic fringe coincident with a given point on the plate, the principal stress directions at that point are immediately given by the inclination of the polariser and analyser axes. Variation of β with respect to unidirectional strain field has also proved critical in strain gauge design. To achieve a maximum intensity β is set to $\pi/4$ [71].

The second condition for light extinction is obtained when the relative retardation is equal to an integer number of wavelengths, i.e (n = 0, 1, 2, 3, ...).

$$\delta = n\lambda \tag{3.13}$$

If the light source used to illuminate the device is monochromatic, for example mercury green or sodium yellow, when this condition is satisfied the resulting spectrum of the fringe pattern appears as a series of distinct black lines on a uniform green or yellow background. However using a polychromatic light white light for example such that generated by a Tungsten Halogen lamp, a continuous range of wavelengths from the ultraviolet end to the extreme red passed through the plate. Since the retardation is a function of the wavelength it may be concluded that the retardation, which causes the extinction of one wavelength does not generally extinguish other wavelengths. Thus the increase of the strain intensity has as a consequence the increase of birefringence magnitude, then each wavelength in the spectrum will extinguish in turn in a sequential manner and the remaining colours being transmitted with smaller or greater intensity according to the nearness of the relative retardation to an integral multiple of their own wavelengths. Therefore, the colour sequence appears for an observer as a complimentary colour. It is this complimentary colour, which makes up the bands of isochromatics, which is apparent with white light. If the region where σ_A, and therefore the relative retardation, is zero is taken as the starting point, thus moving in a direction in the plate in which the stress is increasing, the first fringe to be seen is the black zero isochromatic, then a region where light of all wavelengths is partially restored, i.e. a region faintly illuminated with white light. It should be noted that the colours are extinguished in the order of the colours of the spectrum, beginning with those of shorter wavelength at the violet end [72].

The complete colour sequence, which appears as a result of the satisfaction of the second condition, is given below in Table 3.1. This table includes the relative retardation for each wavelength as well as the fringe order [4, 73].

Colour	Approximate Retardation (nm)	Fringe Order
Black	0	0
Grey	160	0.28
White	260	0.45
Pale Yellow	345	0.60
Orange	460	0.80
Dull Red	520	0.90
Purple	575	1.00
Deep Blue	620	1.08
Blue Green	700	1.22
Green- Yellow	800	1.39
Orange	935	1.63
Rose Red	1050	1.82
Purple	1150	2.00
Blue-Green	1350	2.35
Green-Yellow	1440	2.50
Red	1520	2.65
Red/Green Transition	1730	3.00
Green	1800	3.10
Pink	2100	3.65
Pink/Green transition	2300	4.00
Green	2400	4.15

Table 3.1 - Isochromatic Fringe Characteristic

As can be seen from the above table as the stress increases the colour of the part viewed through the analyser changes from black to yellow to purple. The next colour to be seen with increasing stress is blue, which marks the first fringe order and is often referred to as the ***tint of passage***. Increasing further the stress produces additional retardation that results in the extinction of red and eventually the extinction of violet, thereby extinguishing the colour for the second time.

The result is the combination of two complimentary colours and with each successive complete colour cycle the effect of complex simultaneous extinction is to cause the fringe colours to become paler and less distinctive

3.5 - Introduction to Chromatic Modulation Detection

To detect the spectral sequence, an optical technique based upon the analysis of the dominant wavelength using a double layer of photodiodes has been used. Each layer has a different but overlapping spectral sensitivity $R_{PD1}(\lambda)$ and $R_{PD2}(\lambda)$ (Amperes/Watt). That is, one layer is sensitive to short wavelengths and the other to long wavelengths. This method of detection has many advantages over other techniques; for example, its intensity independence provides immunity to spurious intensity change introduced by other parameters other than that caused by the parameters being measured. Therefore, a complicated stabilisation system can be avoided [74]. Chromatic detection makes available a unified approach to optical fibre based sensing whereby common electronic and optical instrumentation system can be used to detect a wide range of physical parameters [75].

3.5.1 - Tristimulus Detection

The CIE (Commission International d'Eclairage) approach to colour measurement constitutes a solid foundation to any electronic colour measurement system. This method is based upon the principle of trichromatic generalisation which states that over a wide range of conditions of observation, many stimuli can be matched in colour completely by additive mixtures of three fixed primaries stimulus whose radiant powers have been suitably adjusted [76]. The amount of each primary required to generate a particular colour is known as the ***tristimulus value***. The tristimulus function namely x(λ), y(λ), z(λ) that were adopted by the International Commission on Illumination for the various spectrum [77] colours are represented graphically in Figure 3.3.

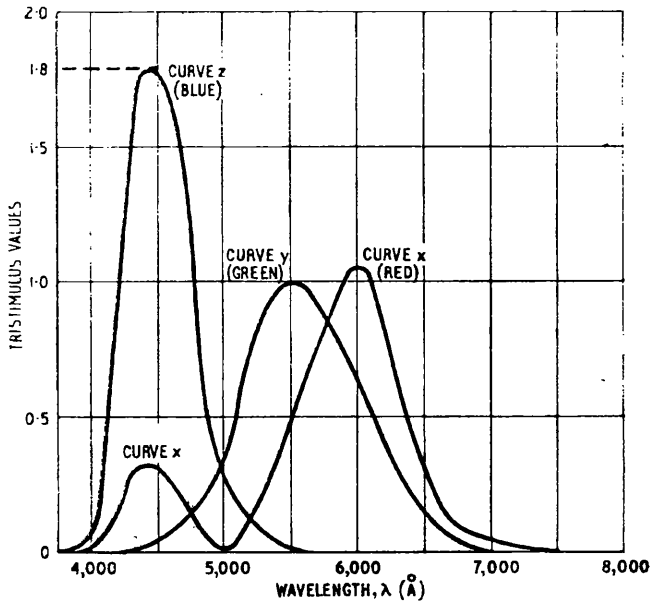

Figure 3.3 - The C I E Standards Tristimulus Functions

If a particular pure wavelength, for instance, λ = 600 nm, produces a colour stimulation S (λ), then:

$$S(\lambda) \equiv X(\lambda) + Y(\lambda) + Z(\lambda)$$
$$S(600) \equiv X(600) + Y(600) + Z(600)$$

Where X (λ), Y(λ), Z(λ) are the amounts of each primary which must be combined to produce a colour stimulation equivalent to S(600).

For a general spectral power distribution, power versus wavelength, P (λ), the tri-stimulus values are found according to Williamson [78]:

$$X = \int_{380nm}^{700nm} P(\lambda)X(\lambda)d\lambda \qquad (3.14)$$

$$Y = \int_{380nm}^{700nm} P(\lambda)Y(\lambda)d\lambda \qquad (3.15)$$

$$Z = \int_{380nm}^{700nm} P(\lambda)Z(\lambda)d\lambda \qquad (3.16)$$

To facilitate the understanding of the colour subject, the CIE recommended a graphical representation of colour in the XY Cartesian coordinates known as the **chromaticity diagram**. This system is often represented as a two-dimensional graphic, which more or less corresponds to the shape of a sail, Figure 3.4 [77]. Each point on the plane defines a colour uniquely, and any two spectral power distributions, which occupy the same point on the plane, will be perceived as the same colour by the human eye. The solid curve that has the horseshoe shaped boundary is the locus of all pure, or saturated, colours from 380 nm to 700 nm.

This locus is determined by computing the chromaticity co-ordinate, x and y from the tristimulus values which are related by the following relationship [80]:

$$x = \frac{X}{X + Y + Z} \qquad (3.17)$$

$$y = \frac{Y}{X+Y+Z} \tag{3.18}$$

$$z = \frac{Z}{X+Y+Z} \tag{3.19}$$

Where X, Y, Z are the tristimulus values, the straight line which closes the curved boundary represents the non-spectral purples. A change in the intensity does not have any influence on the chromaticity coordinates, because, a pure intensity change in P(λ) would manifest itself as a change in the power at all wavelengths by the same amount, say G, and the relative spectral power distribution would become GP(λ). This change would affect each of X, Y, and Z by the same factor and, therefore, the factor G would be cancelled in the formation of the chromaticity coordinates. Thus, a pure change of intensity does not affect the chromaticity coordinates, and therefore, this method of detection provides immunity to intensity change [74, 80].

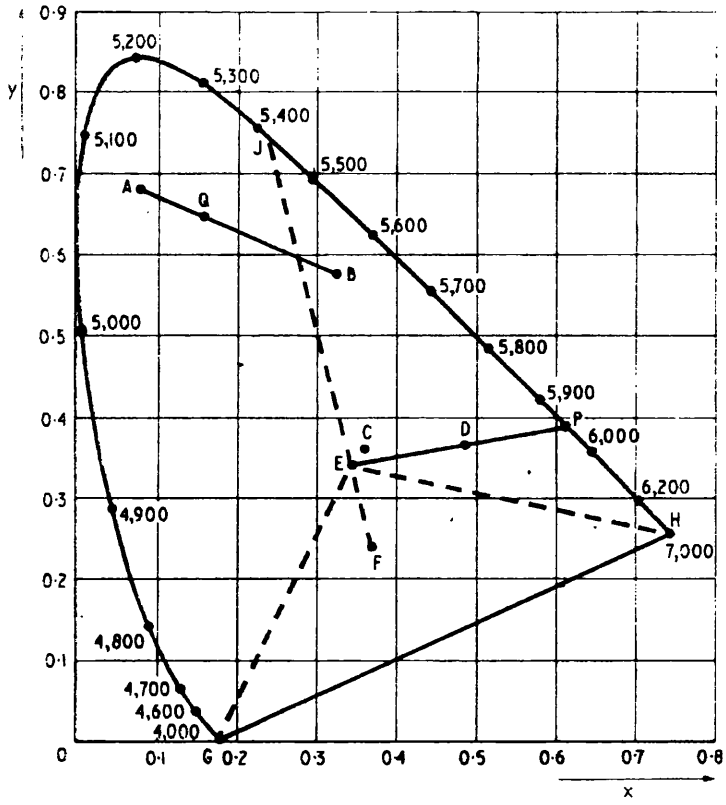

Figure 3.4 - The Chromaticity Diagram for the Spectrum Colour [77]

3.5.1.1 - Dominant Wavelength and Saturation

Colour can also be specified using the chromaticity diagram in terms of dominant wavelength and purity. The most saturated colours are those of the pure colour spectrum and as the colour moves towards the centre of the diagram it becomes less saturated.

The dominant wavelength λ_e, of a colour having as coordinate (x_1, y_1), is determined by drawing a line from the achromatic point through the colour coordinate. The intersection of this line with the locus of the pure colour gives the values of dominant wavelength. Therefore the only difference between a colour with a given dominant wavelength and pure colour of that wavelength is the degree of saturation or mixture with white light. The saturation can be quantitatively defined as the ratio of the distance between the achromatic point and colour position to that between the colour position and the dominant wavelength.

$$saturation = \frac{a}{b} \tag{3.20}$$

Where a and b are the distances of the chromaticity and the perimeter at the dominant wavelength, respectively, from the equal power point. Hence a pure colour has a maximum saturation and is equal to one, whereas white and grey colours have a minimum saturation that is equal to zero.

The coordinates (0.33, 0.33) define the point of a chromaticity where all the greys and white reside. It is called the 'equal power' point because the achromatic colours can be produced by spectral power distributions, which have equal power at all wavelengths. Analytically, the coordinates of achromatic point, (X_w, Y_w) can be

determined by assuming that white light have equal power P_w , thus the tristimulus values [81] become as follows:

$$X_w = P_w \int_{380nm}^{700nm} X(\lambda)\delta\lambda \tag{3.21}$$

$$Y_w = P_w \int_{380nm}^{700nm} Y(\lambda)\delta\lambda \tag{3.22}$$

$$Z_w = P_w \int_{380nm}^{700nm} Z(\lambda)\delta\lambda \tag{3.23}$$

The coordinates of the achromatic point are therefore:

$$x_w = \frac{X_w}{(X_w + Y_w + Z_w)} \tag{3.24}$$

$$y_w = \frac{Y_w}{(X_w + Y_w + Z_w)} \tag{3.25}$$

Finally, drawing a straight line between the extreme points of the pure colour locus closes the colour boundary, which encloses all possible chromaticities. This completes the formation of the chromaticity diagram from the tristimulus functions.

This method of specification cannot be applied however to any point below the achromatic point in the triangle EGH because a straight line from E through F does not intersect the locus of pure colour, but the line GH of non spectral purple. This may be interpreted as that all colours having chromaticity coordinates within the triangle are not desaturated pure colours therefore it doesn't possess a dominant wavelength.

In order to find the dominant wavelength but rather a complementary dominant wavelength, a line is drawn in the opposite direction to intersect with the locus of pure colour. The point intersection thus, determines the complementary wavelength.

In order to appreciate the relevance of this discussion to the problem of electronic multiwavelength detection it is necessary to relate these chromaticity parameters to photodetector currents. That is the tristimulus values may be acquired directly using three photodetectors with spectral responses considered as the tristimulus functions. Unfortunately, standard photodetectors are not usually available with a spectral characteristic similar to that specified by the CIE.

Furthermore; in many applications the chromaticity coordinates may lie in non-visible regions where the CIE system is not operative. This fact dictates the use of photodetectors that do not rigorously provide tristimulus values as defined by the CIE. Therefore, the adapted colour measurement system relies upon the analysis of a chromaticity diagram that results from tristimulus functions, which are defined by photodetector responses. They are analogous but not strictly equivalent to the CIE tristimulus function.

If we consider the incidence of polychromatic light, having a spectral power distribution $P(\lambda)$ (watts/n) on a photodetector (PD1) with a fictitious spectral sensitivity $R_{PD1}(\lambda)$ (Amperes/Watt) (corresponding to the tristimulus function $x(\lambda)$ in Figure 3.3, the short circuit current (Amperes) from this photodetector will be given by:

$$I_{PD1} = K_1 \int P(\lambda) R_{PD1}(\lambda) \partial\lambda \qquad (3.26)$$

Where K_1 is a constant unique to photodetector PD1. Similarly, the short circuit current, for photodetectors PD2 and PD3 is given by:

$$I_{PD2} = K_2 \int P(\lambda) R_{PD2}(\lambda) \partial\lambda \tag{3.27}$$

$$I_{PD3} = K_3 \int P(\lambda) R_{PD3}(\lambda) \partial\lambda \tag{3.28}$$

Where the spectral sensitivities $R_{PD2}(\lambda)$ and $R_{PD3}(\lambda)$ correspond to the tristimulus functions $y(\lambda)$ and $z(\lambda)$ respectively. The chromaticity coordinates for the spectral power distribution $P(\lambda)$ then become:

$$x = \frac{K_1 \int P(\lambda) R_{PD1}(\lambda) \partial\lambda}{\int P(\lambda) . \{K_1 R_{PD1}(\lambda) + K_2 R_{PD2}(\lambda) + K_3 R_{PD3}(\lambda)\} \partial\lambda} \tag{3.29}$$

and

$$y = \frac{K_2 \int P(\lambda) R_{PD2}(\lambda) \partial\lambda}{\int P(\lambda) . \{K_1 R_{PD1}(\lambda) + K_2 R_{PD2}(\lambda) + K_3 R_{PD3}(\lambda)\} \partial\lambda} \tag{3.30}$$

the coordinate z is given by :

$$z = \frac{K_3 \int P(\lambda) R_{PD3}(\lambda) \partial\lambda}{\int P(\lambda) . \{K_1 R_{PD1}(\lambda) + K_2 R_{PD2}(\lambda) + K_3 R_{PD3}(\lambda)\} \partial\lambda} \tag{3.31}$$

The sum of the coordinates x, y and z satisfies the following condition:

$$x + y + z = \frac{\int P(\lambda) . \{K_1 R_{PD1}(\lambda) + K_2 R_{PD2}(\lambda) + K_3 R_{PD3}(\lambda)\} \partial\lambda}{\int P(\lambda) . \{K_1 R_{PD1}(\lambda) + K_2 R_{PD2}(\lambda) + K_3 R_{PD3}(\lambda)\} \partial\lambda} = 1 \tag{3.32}$$

3.6 - Distimulus Detection

The tristimulus detection method upon which colour measurement is based, provides a relatively accurate, intensity independent method of classifying different complex spectral signatures, in terms of their dominant wavelengths and saturation, but, it is technically complicated. In the current application, we are interested in

measurement of dominant wavelength; therefore the use of only two detectors is sufficient.

The distimulus system gives a single output (instead of two output in the case of tristimulus detection); therefore the state of the measurand can be easily calibrated against a single output. In general this dominant wavelength will not be identical to that determined with a three detector system.

In the two detector distimulus system all information related to the colour saturation is lost, therefore a colour with dominant wavelength and a pure colour with the same wavelength cannot be distinguished. In a similar way to that of the tristimulus detection method, derivation can be made for the case of two rather than three photodetectors. In this case the third photodetector is dispensed with ($R_{PD3}(\lambda)=0$) therefore, the chromaticity coordinates will be reduced to :

$$x' = \frac{X}{X+Y} \tag{3.33}$$

$$y' = \frac{Y}{X+Y} \tag{3.34}$$

Where $$x'+y' = \frac{X}{X+Y} + \frac{Y}{X+Y} = 1 \tag{3.35}$$

As can be seen from the above equations, the chromaticity diagram is constrained to a straight line as seen in Figure 3.5.

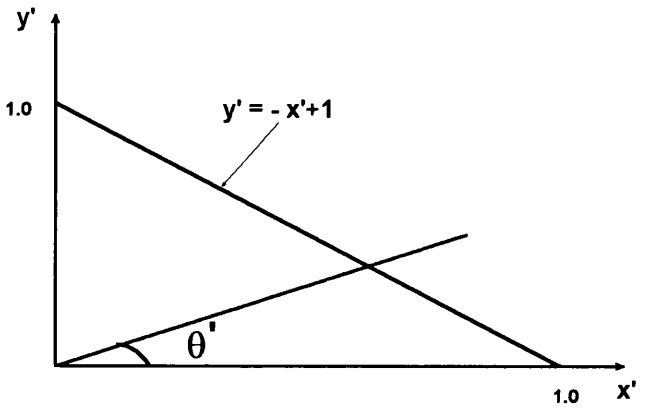

Figure 3. 5 - The Chromaticity Diagram for Distimulus Functions

Either chromaticity coordinate x' or y' may be used to describe completely a distimulus measurement of a spectral signature. As a result the dominant wavelength on a distimulus chromaticity diagram may simply be determined by either of its coordinates x' or y', or by the tan (θ') subtended between the x axes and the line joining the origin to the point (x, y). The tan (θ') can be given by:

$$\tan(\theta') = \left(\frac{x'}{y'}\right) = \left(\frac{X}{Y}\right) = \lambda_e \qquad (3.36)$$

Where λ_e represents the dominant wavelength, and may be determined directly from the ratio of photo detector currents.

$$\lambda_e = \frac{I_{PD1}}{I_{PD2}} = \frac{K_1 \int P(\lambda) R_{PD1}(\lambda) \partial\lambda}{K_2 \int P(\lambda) R_{PD2}(\lambda) \partial\lambda} \qquad (3.37)$$

Where $I_{PD1}, I_{PD2}, K_1, K_2, P(\lambda), R_{PD1}(\lambda)$ *and* $R_{PD2}(\lambda)$ are as specified previously. From this expression the dominant wavelength of a spectrum may be defined. It is clear that λ_e will vary with an asymmetric change in the spectral distribution P(λ), and that this detection is essentially independent of the optical signal intensity for uniform

changes in P(λ). These two photocurrents are practically acquired using two semiconductor photodiodes with a different, but overlapping spectral response corresponding to the distimulus values Figure 3.6. That is one photodiode is sensitive to short wavelength and the second one is sensitive to long wavelength

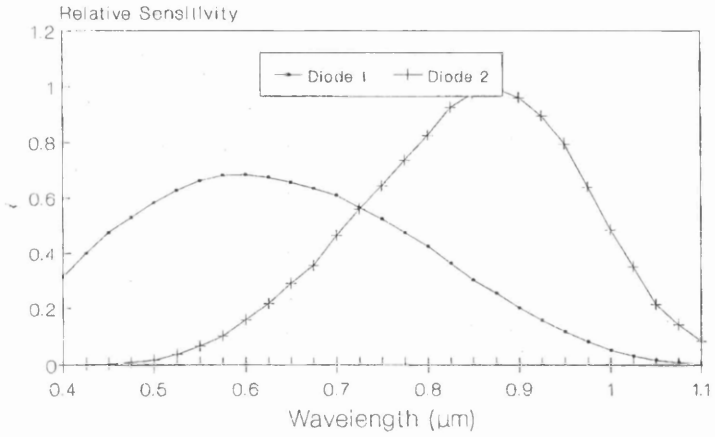

Figure 3.6 - The Spectral Sensitivity of the two Photodiodes

The Sharp PD150 double layer sequential photodiode is used in this application, the schematic diagram is shown in Figure 3.7.

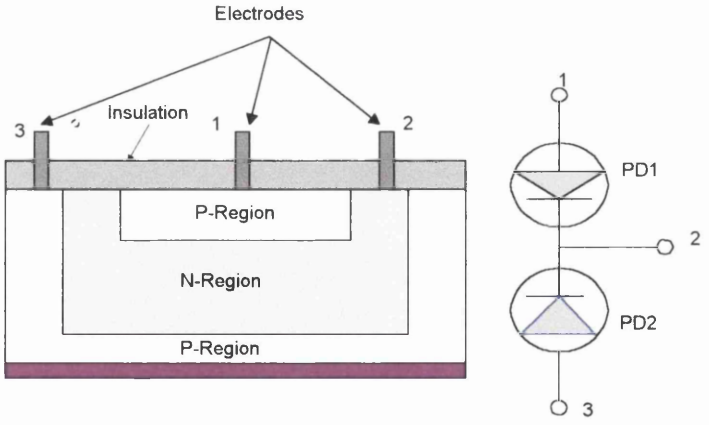

Figure 3.7 - Sharp PD150 Sequential Photodiode

Confining the limits of the mathematical modelling to the defined spectral bandwidth of the PD150 photodetector (Figure 3.6) λ_e may be rewritten in terms of strain, ε, for a spectral distribution I(λ) (Tungsten Halogen Lamp) [66].

$$\lambda_e(\varepsilon) = \frac{K' \int_{400}^{1100} I(\lambda) R_{PD1}(\lambda) \sin^2(2\beta) \sin^2\left\{\frac{\pi\delta}{\lambda}\right\} d\lambda}{K' \int_{400}^{1100} I(\lambda) R_{PD2}(\lambda) \sin^2(2\beta) \sin^2\left\{\frac{\pi\delta}{\lambda}\right\} d\lambda} \tag{3.38}$$

Since the polarisers used in this developed optical strain gauge have an operating bandwidth from 400 nm to 800 nm, equation (3.38) is rearranged to give:

$$\lambda_e(\varepsilon) = \frac{K'\left[\int_{400}^{800} I(\lambda) R_{PD1}(\lambda) \sin^2(2\beta) \sin^2\left\{\frac{\pi\delta}{\lambda}\right\} d\lambda + \int_{800}^{1100} I(\lambda) R_{PD1}(\lambda) \sin^2(2\beta) \sin^2\left\{\frac{\pi\delta}{\lambda}\right\} d\lambda\right]}{K'\left[\int_{400}^{800} I(\lambda) R_{PD2}(\lambda) \sin^2(2\beta) \sin^2\left\{\frac{\pi\delta}{\lambda}\right\} d\lambda + \int_{800}^{1100} I(\lambda) R_{PD2}(\lambda) \sin^2(2\beta) \sin^2\left\{\frac{\pi\delta}{\lambda}\right\} d\lambda\right]} \tag{3.39}$$

Thus for 800 ≤λ≤ 1100 nm:

$$\sin^2(2\beta) \sin^2\left\{\frac{\pi\delta}{\lambda}\right\} = 1 \tag{3.40}$$

Rewriting equation (3.39)

$$\lambda_e(\varepsilon) = \frac{\int_{400}^{800} I(\lambda) R_{PD1}(\lambda) \sin^2(2\beta) \sin^2\left\{\frac{\pi\delta}{\lambda}\right\} d\lambda + A}{\int_{400}^{800} I(\lambda) R_{PD2}(\lambda) \sin^2(2\beta) \sin^2\left\{\frac{\pi\delta}{\lambda}\right\} d\lambda + B} \tag{3.41}$$

Where

$$A = \int_{800}^{1100} I(\lambda) R_{PD1}(\lambda) d\lambda \tag{3.42}$$

And

$$B = \int_{800}^{1100} I(\lambda) R_{PD2}(\lambda) d\lambda \qquad (3.43)$$

It is obvious from equation (3.41) that the output from each photodetector would be a function of $\sin^2$ superimposed upon an unmodulated DC level A (for PD1) and B (for PD2). Moreover since the maximum retardation for photo-elastic stress analysis is ±2400 nm (Table 3.1) therefore, for useful measurements the retardation range used with equation (3.41) was confined to these values. The theoretical response for each of the PD150 photodetectors (i.e. the numerator and denominator of equation (3.41) are given in Figure 3.8 as functions of both positive and negative retardation. The negative retardation values are deduced by symmetry.

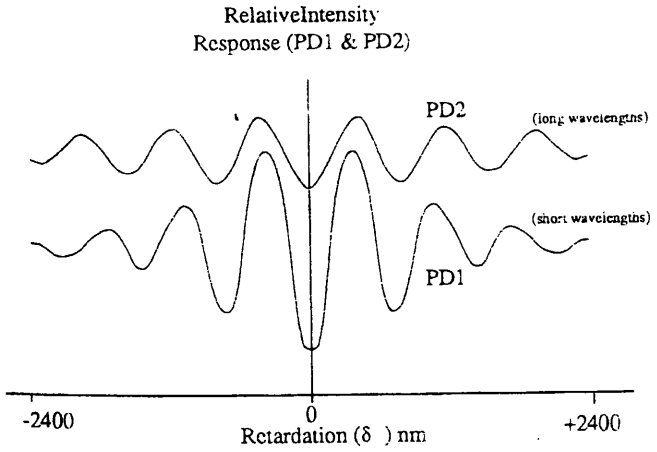

Figure 3.8 - The Theoretical Response of the two Photodiodes

The corresponding theoretical variation of the chromatic transfer function $\lambda_e(\varepsilon)$ (equation (3.41) is given in Figure 3.9.

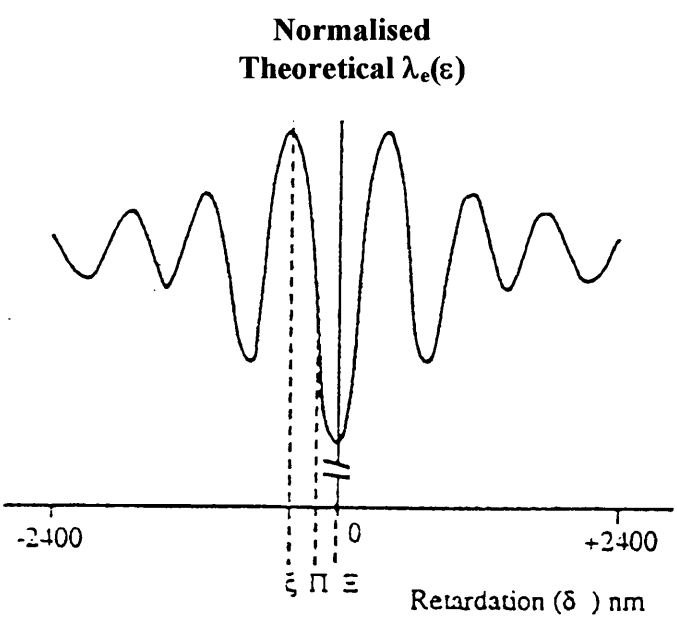

Figure 3.9 – Photo Detector Ratio (Normalized (Theoretical $\lambda_e(\varepsilon)$))

By virtue of the $\sin^2(\delta\pi/\lambda)$ term in both the numerator and denominator of equation (3.41) then irrespective of the sign of the retardation (or uniaxial strain) this term will always remain positive. Indeed, the plot of the theoretical transfer function does show symmetry for both positive and negative retardation with respect to the zero point. Furthermore these results show that over the given range of retardation the uniaxial strain magnitude, if determined (Figure 3.9), from the relative chromatic response would be multivalued for $\delta>\varepsilon$. The symmetry about point zero (δ, ε= 0) leads to ambiguity as to the sign of this strain. Consequently, the dynamic range of the device needs to be restricted between the range ξ and Ξ and the zero strain point must be set at Π in order that the sign of the strain may be determined (tension or compression).

In order to meet these criteria the most critical requirement is to shift the zero point (δ, ε=0) Figure 3.9 from $\delta=\Xi$ to $\delta=\Pi$. As it can be seen from Figure 3.9, the overall retardation from ξ to Ξ is approximately equal to 300 nm, which would suggest that a further retardation of 300/2 = 150 nm should be introduced in order to move the zero

strain point to Π. Therefore, an optical element that can induce the required retardation needs to be introduced into the optical system.

As it is well known, the phase difference that can be induced by a quarter wave-plate is usually equal to one quarter of a wavelength for green (560 nm) monochromatic light i.e. (140 nm). It is obvious that this form of filter experiences approximately the same retardation, as that required for the dislocation of the strain zero point to the approximate position of Π. Therefore, with the inclusion of this retardation in the system scheme, an additional retardation ($\Delta \approx \pm 140$ nm) can be added to the initial one so that equation (3.10) becomes:

$$I = \sum_{\lambda} I_{\lambda} \sin^2(2\beta) \sin^2\left\{\frac{\pi(\delta + \Delta)}{\lambda}\right\} \tag{3.44}$$

In the current application the circular polarising filter HNCP37 [Optical Filters Ltd., 1990] was introduced in a hybrid combination of linear and circular mode, which results in the emergence of light as left-handed circularly polarised light. That is the electric vector component $E_x(t)$ leads the component $E_y(t)$, and Δ is defined in terms of e by the expression [polaroid, 1990]:

$$\Delta(\text{nm}) = -\left\{\frac{e}{2\pi}\right\}\lambda \tag{3.45}$$

Where λ is, the wavelength of green light, 560 nm.

The origin of the negative term in equation (3.45) arises from the convention used in this work - that is the fast axis $E_x(t)$ leads the slow axis $E_y(t)$ by $\pi/2$. Therefore since a positive uniaxial stress (and hence strain) introduces a positive retardation and

retards polarisation components by δ parallel to this stress direction, then the sign of any phase change (e) will be negative. Of course for a negative uniaxial stress (and so strain), then the converse is true. A complete coverage of the gauge design criteria is well documented by other authors (M. Murphy's PhD thesis university of Liverpool 1991). In this current application we are limited to mentioning them briefly.

The alignment transmission axis of the polariser with respect to the direction of principal strain has been proved to be critical for strain gauge design. In order to achieve a maximum gauge sensitivity and great modulation depth, the transmission axis needs to be set at $\frac{\pi}{4}$ to the direction of principal strain Figure 3.10.

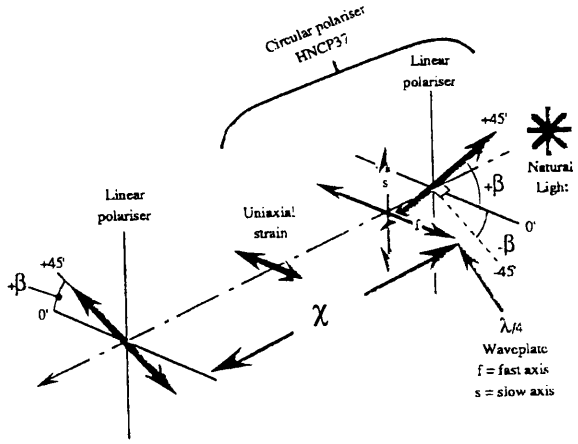

Figure 3.10 - Optical Arrangement Showing the Angle β for Crossed Linear/Circular Polariser Arrangement

As it can be seen from Figure 3.10, the fast axis of the quarter-wave plate is parallel to the direction of uniaxial strain; consequently this component when it reaches the optical gauge will become retarded under the influence of the stress. The slow axis,

which is orthogonal to the fast axis, is not under stress, therefore, the polarisation component propagating along this axis experiences no change in velocity on entering the optical strain gauge. However, the first component i.e. along the fast axis initially leads that parallel to the slow axis by $\pi/2$, therefore, the increase of the strain results in the reduction of the overall retardation between these two polarisation components. As the strain is further increased a point where the overall retardation will be zero is reached, and the linear polarisation state will be perpendicular to the analyser-transmitting axis. Consequently, no optical disturbance is transmitted giving the dark field condition.

The corresponding strain magnitude determines the maximum positive strain that can be measured. The circular polariser transmission axis alignment is not critical with respect to the optical components constituting the optical strain gauge. However, it has been shown that sensitivity is 10 % greater for an orientation of 0° compared with an orientation of 90°. Planar twisting has a significant effect on altering the sensitivity of the strain gauge when the quarter-wave plate is caused to tilt about its fast and slow axes. For small planar misalignment (smaller than 10°) the change in retardation is too small to be of any concern in optical gauge construction.

A formal design of an optical strain gauge replicating the required optical adjustments mentioned above was constructed and delivered by Lucas engineering company. This satisfied the initial specifications with respect to the induced retardation requirement and the critical alignment of the polarisers for optimised gauge performance. The polarisers used were polymeric operating in linear and circular mode and the sensing axis of the strain gauge was, of course, orthogonal to the direction of light propagation.

In overcoming the problems associated with initial birefringence and to develop an optical gauge, which would not require skilled intensive labour for its construction, a casting process was implemented. A thermosetting optical epoxy was selected which has a suitable Young's modulus and strain-optic coefficient. The construction of this device is given in Figure 3.11. The polarisers are bonded within the polymeric unit, enabling remarkable device rugedness and overcoming foreign body ingress.

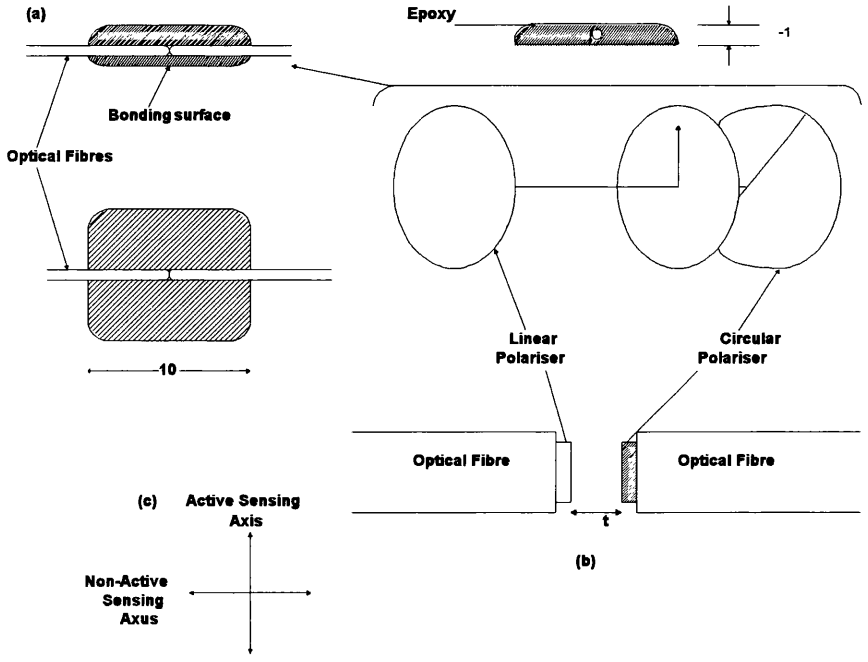

Figure 3.11 - Configuration of: (a) The Casting Unit (b) Cast Optical Strain Gauge in Third Angle Projection Showing (c) Active Element Detail Sensing Axes

3.7 – Conclusion

The design criteria of an optical strain gauge based upon photo-elasticity have been described and outlined. It has been shown that the transmission axis of the polariser must be set at an angle equal to $\pi/4$ to achieve a maximum sensitivity. A quarter

wave-plate is introduced in the optical arrangement to shift the retardation corresponding to zero strain point by 150 nm in order to determine the sign of the strain (tension or compression). The construction of the gauge is made possible through a casting process to avoid problems related to the initial birefrengence that can be introduced during machining techniques. A double layer photodiode each having different but overlapping spectral sensitivity is used to detect the output signal.

CHAPTER 4

EXPERIMENTAL WORK

4.1 - Introduction

There are two methods currently in use to detect the chromaticity of the returned spectra; namely, logarithmic measurement of the dominant wavelength and the linear distimulus measurement system. In the former method, a logarithmic function proportional to Log (tan (θ')) is obtained; whereas for the latter method a linear function of tan (θ') is obtained. The linear distimulus measurement system is used in this application because of its simplicity. The experimental set-up is outlined and the main block diagrams are described. The design details of the detection system are given. The validity of the proposed optical sensor is evaluated and its performance is critically analysed. Practical tests were carried out. These are the static tests, dynamic tests and repeatability tests. The practical results are then related to the theory. Finally some concluding remarks are given at the end of this Chapter.

4.2 - Linear Distimulus measurement system

The Sharp PD150 [80] double diode with a common cathode is used. It consists of two photodiodes PD1 and PD2 in a single substrate as described in Chapter 3, section 3.6. PD1 and PD2 have a short and long wavelength sensitivities respectively as shown in Figure 3.6. This double diode is embedded in the SMA connector as depicted in Figure 4.1.

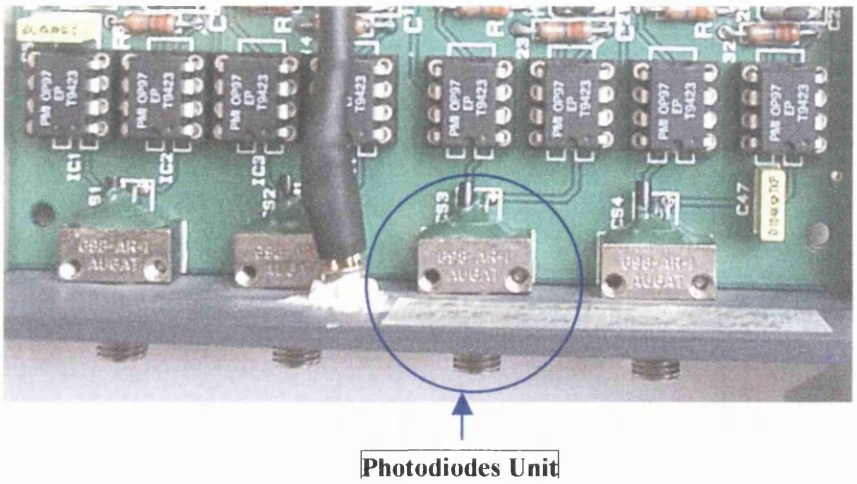

Figure 4.1 - Four Channel Detection Board

The output photocurrents I_{PD1} and I_{PD2} from the two photodiodes are converted into voltages using transresistance operational amplifiers as shown by Figure 4.2. An output function, V_{out}, proportional to tan (θ') is produced by dividing these two voltages.

The transfer function of the linear distimulus measurement system is given by the following equation:

$$V_{out} = G\left(\frac{I_{PD2}R_{f2}}{I_{PD1}R_{f1}} - V_{off}\right) \qquad (4.1)$$

Where V_{out} is the equivalent chromatic transfer function, which is proportional to tan (θ'), G is a gain factor, I_{PD1} and I_{PD2} are the photocurrents i.e., the outputs of the photodiodes 1 and 2 respectively. R_{f1} and R_{f2} are the transresistance amplifier feedback resistor values, and finally V_{off} is an offset.

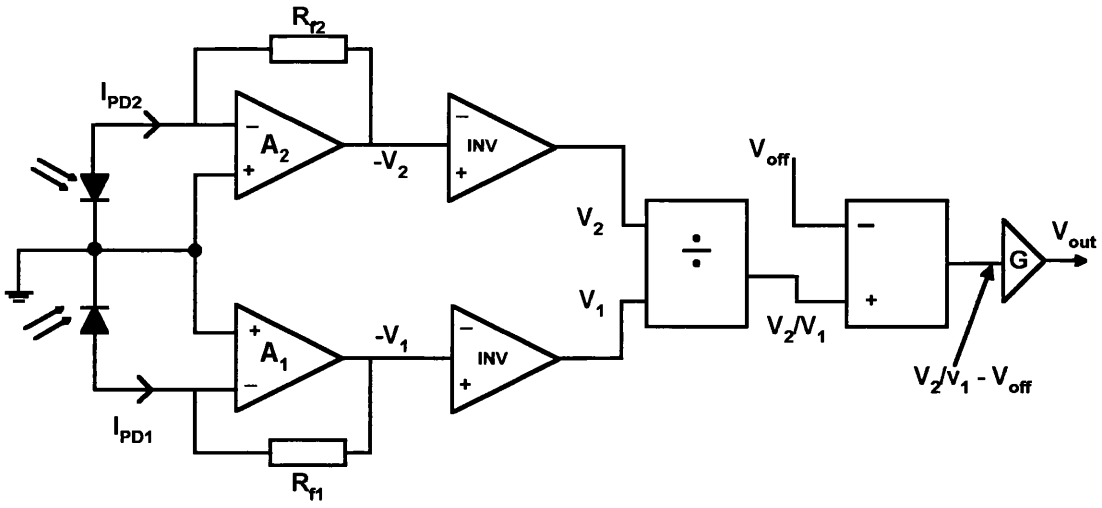

Figure 4.2- Block Diagram of the Detection System

Certain conditions are required in order to fulfil the correct operation of the linear detection technique, which are:

1. A minimum operational light intensity of 1.5 $\mu W/m^2$ (or a minimum operational photocurrent of 1500 fA) forms the threshold for the detection,

2. Since the divider takes the ratio of the two photodetectors currents then in order to avoid voltage saturation, it is necessary to ensure that the numerator is always less than the denominator,

3. It has been determined that the linear processing system has a resolution of ± 0.0095 nm.

Generally, optoelectronic systems are susceptible to output drift related to the ambient temperature variation therefore, account must be paid for the temperature coefficient of the PD150. Indeed the temperature drift originating in the sequential photodiode (PD150) was found to be equivalent to an error in the dominant wavelength measurement of 0.4 nm/°C.

As stated above the linear detection system has a resolution of ± 0.0095 nm. Therefore in order not to further limit the system performance, a system that is able to keep temperature constant to at least ± 0.0095 / 0.4 = ± 0.024°C is needed. In order to keep the temperature of the photodiode constant to within ± 0.024°C over an ambient temperature change as large as 10°C, the photodiode is mounted on a heat sink.

4.3 - Digital Implementation

In order to obtain the ratio between V_1 and V_2 in digital format an analogue to digital divider was used. Based on the AD574AJN, which uses the successive approximation technique. Its basic architecture [82] is shown in Figure 4.3.

A typical successive approximation ADC consists of three, main components, a comparator, a DAC and a control counter and the successive approximation register (SAR). V_{in} is the analogue input voltage to be converted into a digital format, V_{ref} is an analogue reference voltage and V_d is the DAC output voltage.

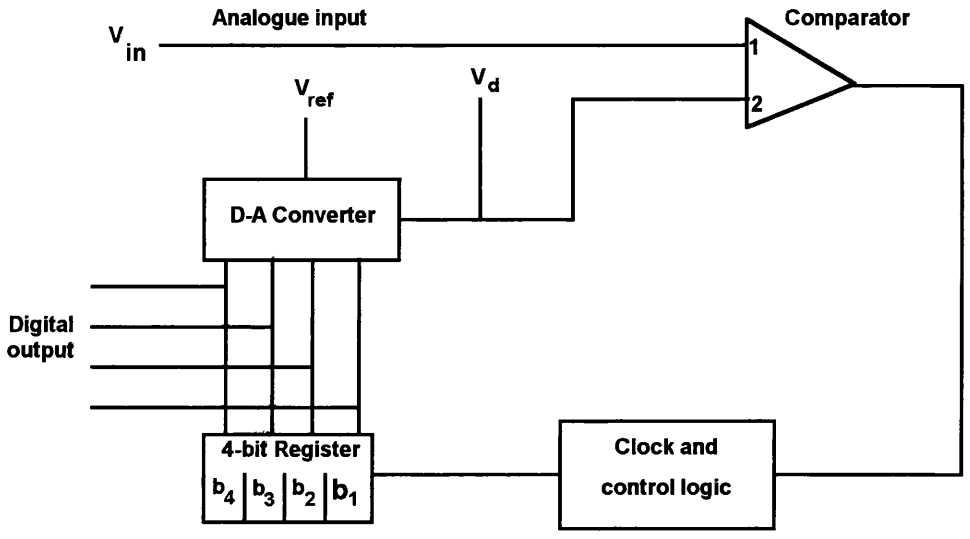

Figure 4.3 - Successive Approximation ADC

At the start of the conversion the first clock pulse clears all the register outputs to logic zero. On the second clock pulse the most significant bit of the latch is set to one causing the DAC output to change to half of its maximum value. This value is compared to the input voltage V_{in}. If the analogue input is higher than the DA converter output, the comparator output causes the logic control to leave the register bit set to one. If however, the analogue input is less than the DA output then the latch bit is reset to zero. On the next clock pulse this process is repeated for the next most significant bit, and so on until all the bits of the latch have been tested. At the end of conversion, the state of the latch bits gives the ADC digital output.

As previously stated, the successive approximation ADC essentially equates a voltage from a DAC to the input voltage V_{in}, and the digital output from the ADC is given by the latched output of the counter, Figure 4.3.

Equation (4.2) gives the input voltage of the DAC in terms of the reference voltage, V_{ref}, the number of DAC bits, n, and the binary DAC input value, b.

$$\frac{V_{in}}{V_{ref}} = \frac{b}{2^n} \tag{4.2}$$

The value b completely describes the ratio V_{in}/V_{ref} since the number of ADC bits, n, is constant. Thus the ADC is used as a digital divider.

$$\frac{V_{in}}{V_{ref}} \alpha\, b \tag{4.3}$$

Where V_{in} is equivalent to $G(V_2-\alpha V_1)$ and V_{ref} is equivalent to V_1

Substituting the values of V_{in} and V_{ref} in equation 4.3 leads to a linear equation of the form y = mx + c where m is the slope of the line and c is the offset. This feature is explored in the next sub-sections

4.3.1- Photocurrent Pre-processing Prior to Division

Two operations must be performed on the photocurrents, generated by the photodiodes in response to incident light, in order to make them ready for division by the ADC Firstly the photocurrents are converted into voltages, by trans-resistance amplifiers. Secondly the voltages are processed in such a way as to make the most efficient use of the operating range of the ADC.

The linear chromatic modulation measurement system uses a post processing stage to select and amplify a specific range from the divider output. For a digital divider system, the range selection and amplification must occur before the ADC division takes place, as the number of ADC bits fixes the accuracy in the digital output. To achieve a range selection and amplification pre-processing system for ADC division the following transfer function, equation (4.4), was chosen:

$$V_{out} = \frac{G(V_2 - \alpha V_1)}{V_1} \qquad (4.4)$$

Where G and α are independent gain factors, V_1 and V_2 are the transresistance stage output voltages derived from the photocurrents, I_{PD1} and I_{PD2}.

V_{out} is independent of optical intensity; in common with the CIE chromaticity coordinates. However, V_{out} is designed to represent a shift in tanθ, from an initial value in the measurand (for which typically α is chosen such that $V_2 = \alpha V_1$ and

$V_{out} = 0$) to some new value, representing the current measurand state. This form of equation is useful in chromatic systems where the dominant wavelength of the special signature varies monotonically with the measurand. The advantage of using equation (4.4) with the ADC divider is that the gain factors may be altered in order to cover the whole output range of the ADC for a given change in chromaticity (or dominant wavelength). For high gains, the accuracy of the ADC will be a function of the noise levels present in both V_1 and $G(V_2-\alpha V_1)$.

4.3.2 - The Pre-Processing Circuit

The numerator and denominator of equation (4.4) (V_1 and $G(V_2-\alpha V_1)$) can be practically acquired by using four operational amplifiers as illustrated in the circuit shown in Figure 4.4.

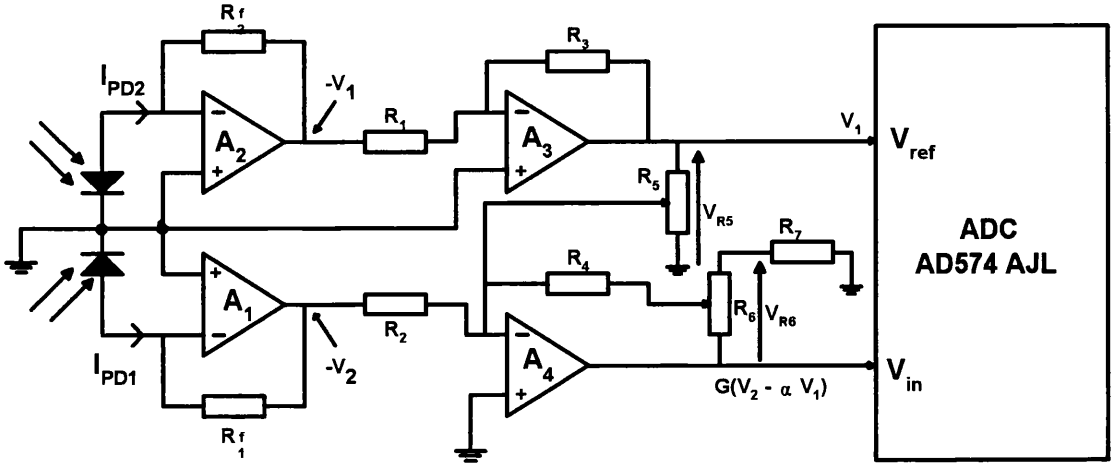

Figure 4.4- Schematic of the Pre-processing Circuit

The photocurrents generated by the photodiodes are first converted into voltages using transresistance amplifiers A1 and A2. The output from a transresistance amplifier is negative; therefore it needs to be inverted (A3, A4) before division will be carried out. To perform this division an amplifier having a fixed gain factor equal

to -1 is used. A small portion, α, of V_1 is obtained from the potential divider V_{R5}. The voltage αV_1 is summed with $-V_2$, and the result amplified by a factor -G, set using V_{R6}, to give a result $G(V_2-\alpha V_1)$.

The two voltages V_1 and $G(V_2-\alpha V_1)$ are fed to the 12-bit AD574AJN ADC terminals at V_{ref} and V_{in} respectively. The design of the pre-processing circuit must take into account the limitation of the voltage ranges of V_{in} and V_{ref} so that saturation can be avoided the limits are set below:

$$5V \geq V_{ref} \geq 1V \text{ and } V_{ref} \geq V_{in} \geq 0 \qquad (4.5)$$

Since the linearity of the proposed optical strain gauge sensor is of paramount importance, equation 4.2 must be tested with AD574 ADC.

The value of V_{ref} was varied from 1V to 5V and the value of V_{in} was varied in steps of 0.5V in the allowed range. The ratio of V_{in}/V_{ref} against the corresponding binary number, b was plotted as shown in Figure 4.5. This clearly shows the linearity required by the proposed system requirements.

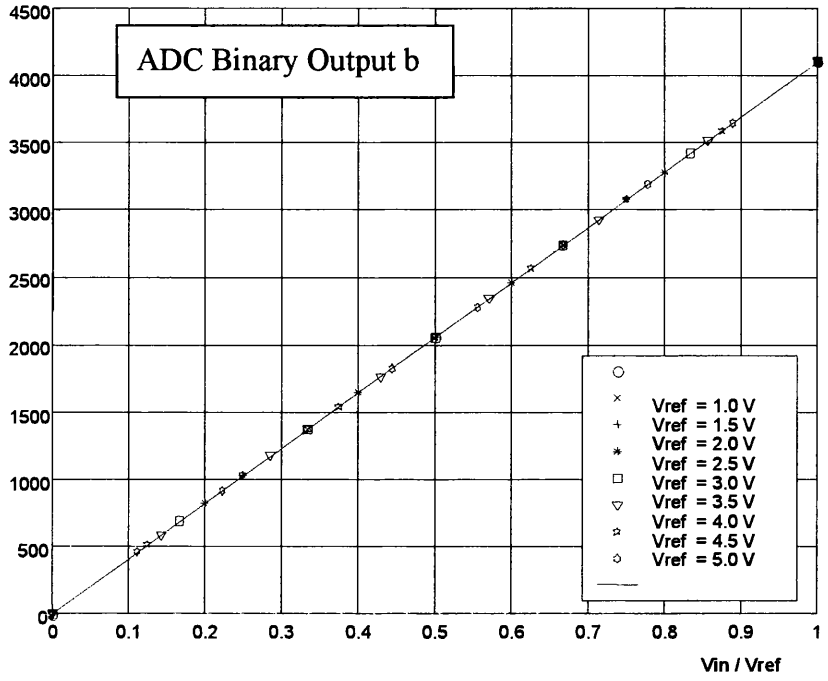

Figure 4.5 The Use of an AD574 ADC as Divider

The pre-processing circuit components list and values are given in Table 4.1. It should be noted that in Figure 4.4 the power supplies, and de-coupling capacitors are omitted for clarity.

Components	Values
R_{f2}	1MΩ
R_{f1}	1MΩ
R_1	10kΩ
R_2	10kΩ
R_3	10kΩ
R_4	10kΩ
R_5	1kΩ
R_6	10kΩ
R_7	100Ω

Table 4.1: Components Values

4.4 - Overall System

The proposed optical sensing system to monitor on-line the contact force consists of an 8- channel optical source module, a 4-channel detection module and an optical strain gauge as shown in Figure 4.6.

A transmitting optical fibre conducts a light signal generated by a Tungsten-Halogen lamp emitting white light to the sensing area where interaction between this signal and the measurand i.e. the contact force takes place, then the modulated signal is launched into a transmitting fibre within which it is guided to the detection module as described in the above section.

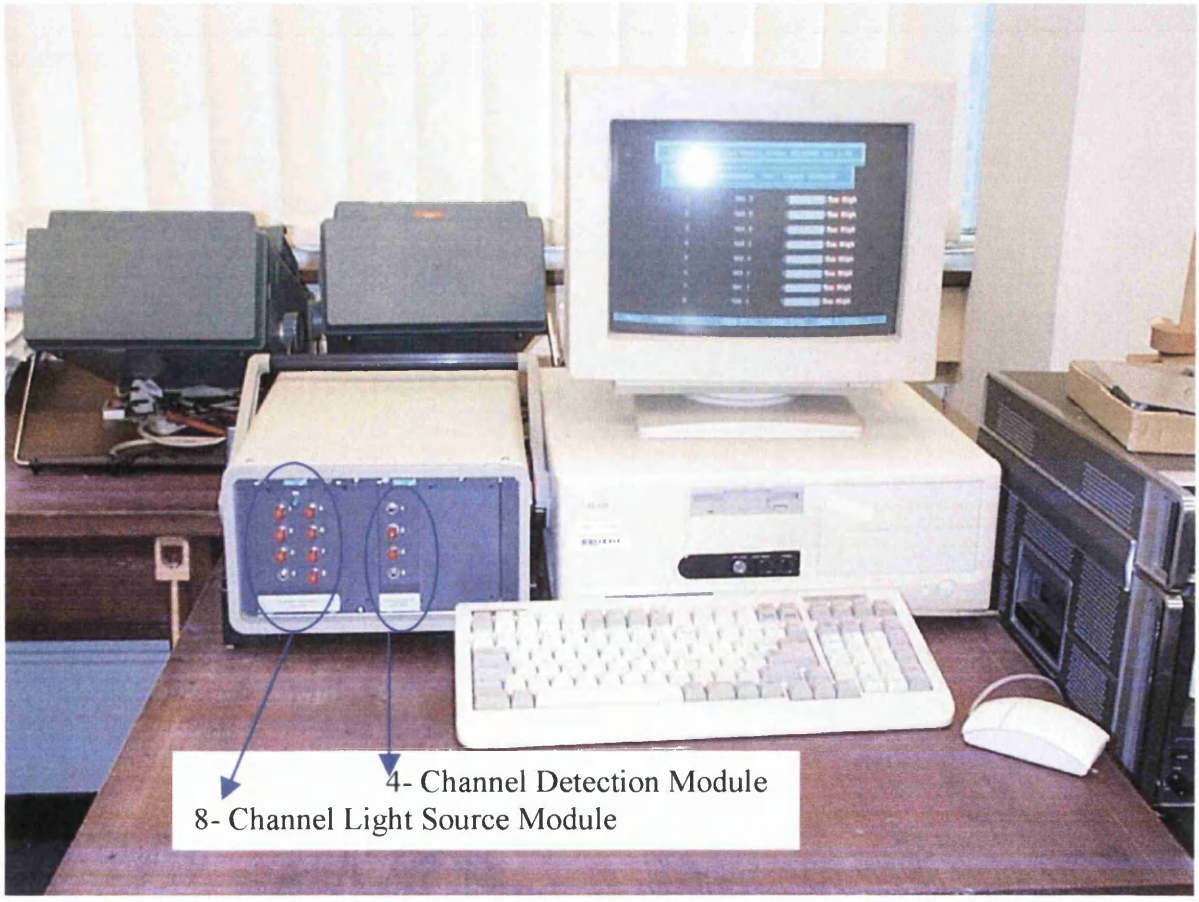

Figure 4.6 - Optical Strain Gauge System

The optical rack system, as shown in Figure 4.7, can be driven as follows:

The first step that has to be performed to drive the optical sensor rack system is to select a channel to determine which input performs the required sensing process. Channel selection is performed by writing a binary word 'xx1100nn' at the address 0x300 where "xx" states are undefined and "nn" states are the inputs defined in Table 4.2.

The second step is an automatic gain control. The minimum gain is assumed by writing 11001001 to address 0x302. The third step is to place the S/H device into hold mode by writing 'xx100nn' to address 0x300. Subsequently, write anything to address 0x301 to start an 8-bit conversion, and then wait for a period of time of about 13 μs in order that the MSBytes of address 0x303 becomes zero, and read the content of address location 0x300.

If the result found is less than that of address 0x8C then proceed to increase the gain by returning to step number two but this time by writing 10001001 rather than 11001001 to address location 0x302. This procedure must be repeated until the result read exceeds that of 0x8C, but this time using '01001001' and '00001001' for progressively more gain.

The routine should be built up in such a way as to set the gain reading of every input to the PC because it is not possible to read the setting back from the module. Subsequent calls to this routine can then check for correct intensity and adjust the gain up or down according to the result of the test greater or equal to 0xFE as the condition to reduce the gain.

This gain setting routine should be called on a regular basis to make sure that the gain reflects any changes in received light intensity. Once this gain is set correctly the

strain reading can be taken as follows. Write 'xx1110nn' to address 0x303 to select the input, colour measurement and sample mode. Wait at least 10 μs then; write 'xx1010nn' to address location 0x303 to put the S/H amplifier in hold mode.

nn	Channel No
00	Input number 1
01	Input number 2
10	Input number 3
11	Input number 4

Table 4.2- Input Channel Number

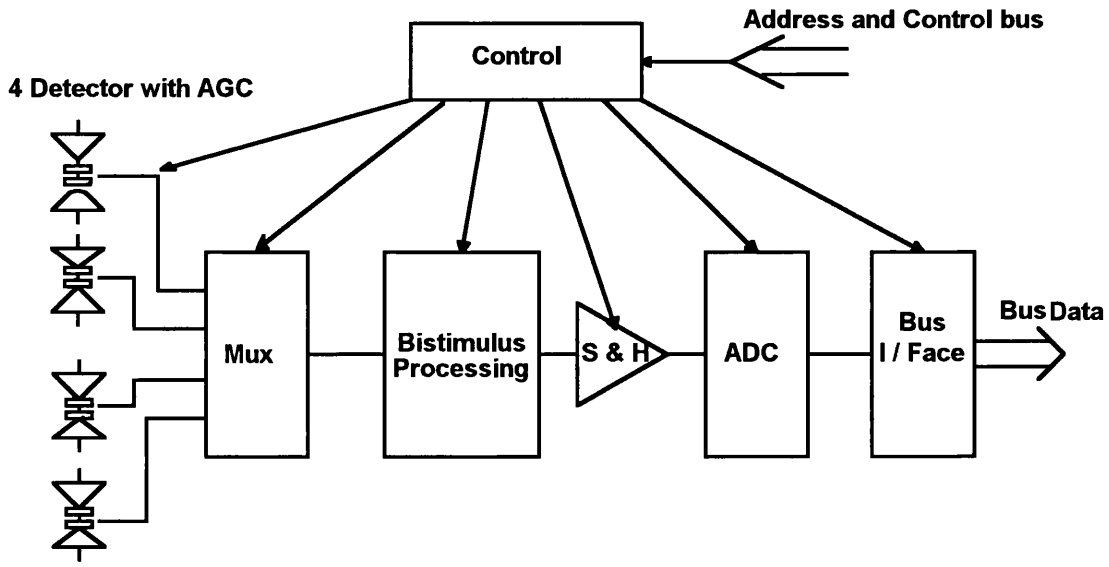

Figure 4.7 -A Simplified Schematic of the Distimulus System

The following step is to write anything to address 0x300 in order to start a 12 bits conversion, and then wait nearly (20 μs), in order that the MSBytes of address 0x303 becomes 0 and read the addresses 0x300 (MSBytes) and 0x301 (LSBytes). The sum

of MSBytes and LSBytes gives a 16 bits integer but with 12 bits resolution, i.e. the four LSBytes are always zero. From this reading a derivation using the look-up table given in appendix A can be made possible to determine the corresponding dominant wavelength.

The look-up table can be used in the following way. The result of the division of the MSBytes of the colour reading by four is used to determine the corresponding row (index). The first value of each row is 16x slope of this region of the curve, and the second value is the offset at the start of this region, the third value in the row can be ignored. The formula to convert is then:

$$Index = V_{off} + \frac{[\mathrm{Re}sultMod[16]] * slope}{16} \qquad (4.6)$$

According to the steps outlined above to drive the rack system, a program written in C language is developed, it displays the dominant wavelength and tracks any change of wavelength when a force applied to the transducer varies. The program and its flowchart are appended in appendix B and appendix C, respectively.

4.5 - Static Test

The optical strain gauge is subject to an applied force of a known magnitude. The gauge is fixed upon a piece of metal mounted on the table by clamps. A hanger upon which the force is applied is positioned on the gauge perpendicular to light propagation direction, providing a point contact with the active area of the optical strain gauge. The load is first slowly increasingly varied from 0 N up to 150 N. A computer system performing the automatic gain control is used to read the data from

the optical sensor system and displays the dominant wavelength corresponding to the magnitude of the applied load Figure 4.8.

In order to determine how much hysterisis the transducer exhibits the applied load is continuously removed. That is, the load is progressively reduced after it reaches the maximum value of 150 N passing by the same steps as when the load was increased. The test results are tabulated in Table 4.3 and plotted on Cartesian coordinates Figure 4.9. The x-axis corresponds to the applied load; the y-axis corresponds to the returned dominant wavelength.

As can be seen from Figure 4.9, the dominant wavelength increases when the load is increased but, after certain value in this case 80 N, the dominant wavelength decreases as the force is further increased therefore only one dominant wavelength may correspond to different magnitudes of a force, this is in agreement with the theory as explained in section 3.6. As a consequence of this, the measurement range of the force should be limited in the range of 0 to 80 N i.e. in the linear range.

Figure 4.8 - Experimental Set-up of Static Test

Force (N)	Wavelength increasing load (nm)	Wavelength decreasing load (nm)
0	854.3	854.9
5	855.6	856.3
8	856.5	857.1
13	858.1	858.8
15	858.9	859.7
20	860.5	861.3
30	863.4	863.9
35	864.9	865.9
40	865.9	867.6
50	869.4	870.1
70	875.6	876.8
80	878.6	879.2
90	878.5	878.1
100	876.7	876.2
120	869.9	870.3
130	872.3	873.9
150	866.9	867.6

Table 4.4 –Results of the static test

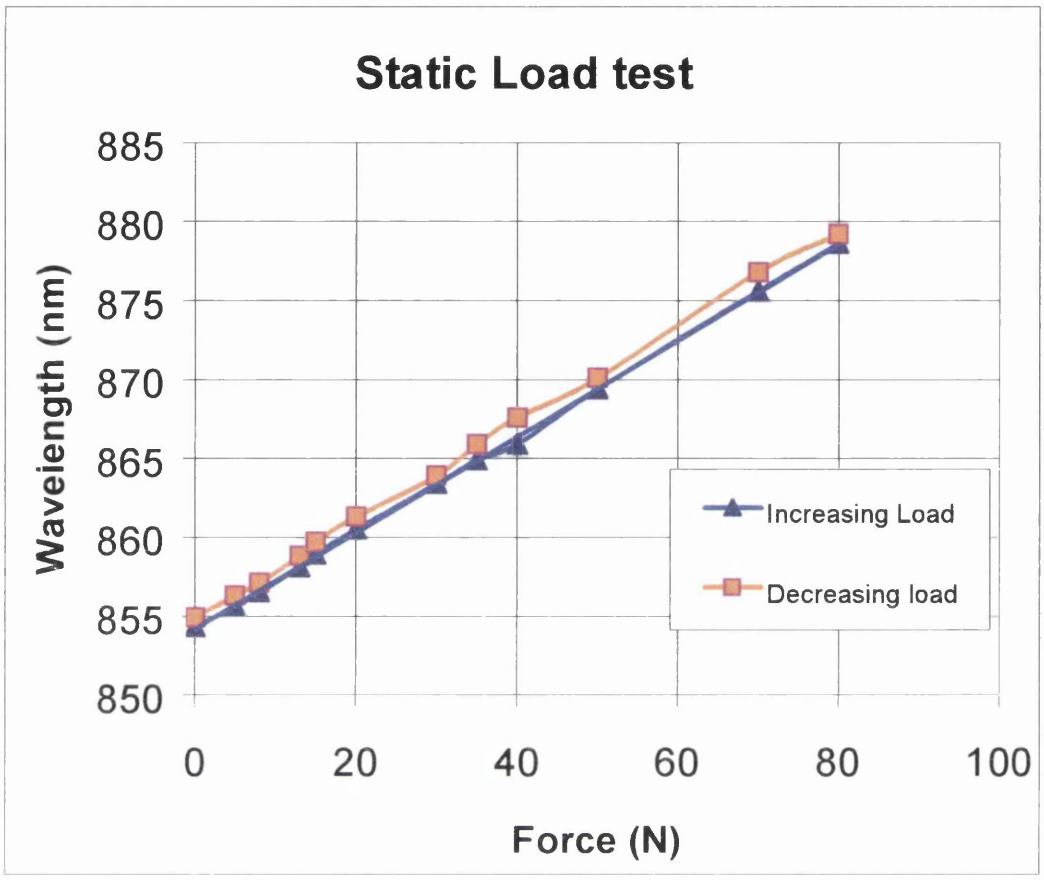

Figure 4.9 –Response of the Strain Gauge to a Static Load

It can also be seen from Figure 4.9 that there is a small amount of hysterisis. It means, that all the energy put into the stressed part while loading is not completely recoverable while unloading.

The amount of hysterisis exhibited may arise from the non-perfect positioning of the hanger on the active region of the photoelastic material (it is practically impossible to realise a point contact). The major factor contributing to such an effect is the physical nature the material of the strain gauge.

A load generated by the hanger may cause the slight departure of the optical response of the strain gauge from linearity. This load is sufficient to pre-strain the optical strain gauge. Moreover, additional stresses induced during clamping may contribute also to strain gauge pre-strain. In addition, the type of connectors used and the positioning of the optical source relative to the tip end of the optical fibre may also be a contributing factor.

4.5.1 – Repeatability

In order to determine the repeatability of the current strain gauge a series of measurements were repeated over a number of days under the same conditions Table 4.5. It has been found that the system has a high repeatability Figure 4.10. The slight defect could be attributed to the fluctuation of the temperature or systematic errors.

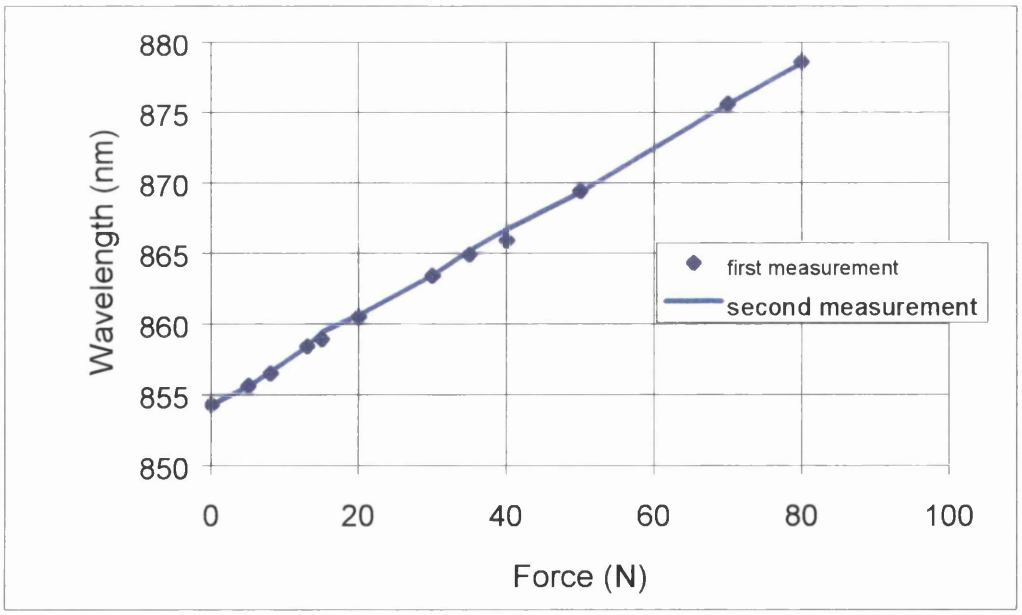

Figure 4.10 – Plot of the Experimental Results of the Repeatability Test

Force (N)	Wavelength increasing load (nm)	Wavelength decreasing load (nm)
0	854.3	854.8
5	855.6	856.3
8	856.6	857.1
13	858.4	858.9
15	859.4	860.1
20	860.6	861.3
30	863.4	863.9
35	865.2	865.9
40	866.7	867.6
50	869.3	870.1
70	875.6	876.1
80	878.5	879.2
90	878.3	877.9
100	876.7	876,3
120	869.8	870.4
130	872.3	873.8
150	866.9	867.5

Table 4.5 - Experimental result of repeatability test

4.6 - Dynamic Test

Ideally the developed optical strain gauge sensor should be mounted on the pantograph and tested. However, this is beyond the scope of this project, as it is envisaged that once the feasibility of the proposed sensor is complete, the industrial partners will develop the project further to be tested on an electrical train, as many other requirements must be met.

In the application sought, the optical strain gauge will be subjected to dynamic forces as the overhead line makes contact with the pantograph, therefore the developed optical strain gauge must be tested for resistance to these dynamic forces. The Hounsfield dynamic test machine capable of testing samples for strain, stress and many other parameters, is used to test the optical sensor. Using the machine shown below (Figure 4.11), the current optical strain gauge was firstly subjected to a dynamic force of maximum value of 200 N (Figure 4.12) then to rapidly time varying force of maximum value of 300 N (Figure 4.13) The optical strain gauge was mounted between two flat metallic pieces. The top one served as a means of applying a compressive force, the computer controls its displacement towards the strain gauge, as it gets closer to the strain gauge the magnitude of the force is rapidly increased. The computer serves also as data logger.

The optical strain gauge has demonstrated a large resistance to such dynamic forces. The graph of the dynamic force as a function of the dominant wavelength is not plotted because the machine develops forces as a function of displacement rather than time. Moreover, the speed of exerting the force is not constant.

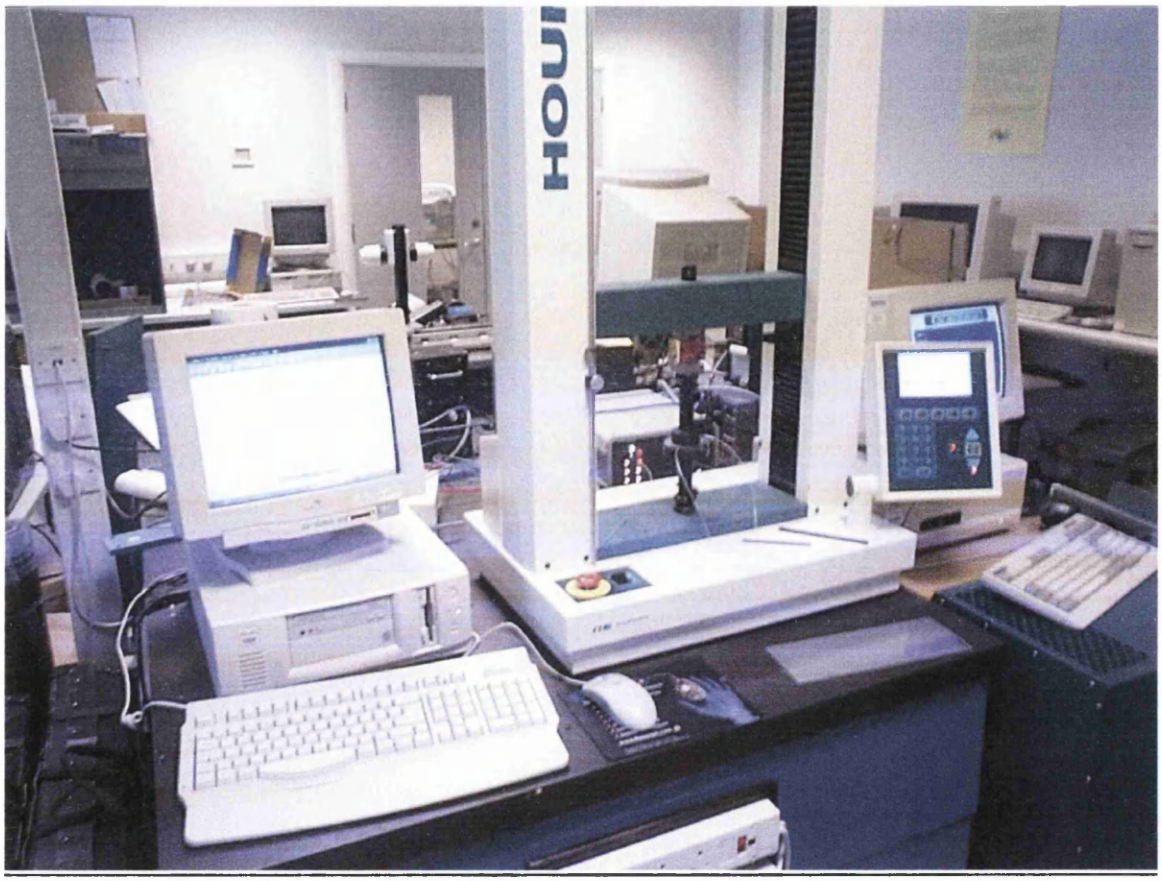

Figure 4.11- Dynamic Test Experimental Set-up for the Compressive Force Test

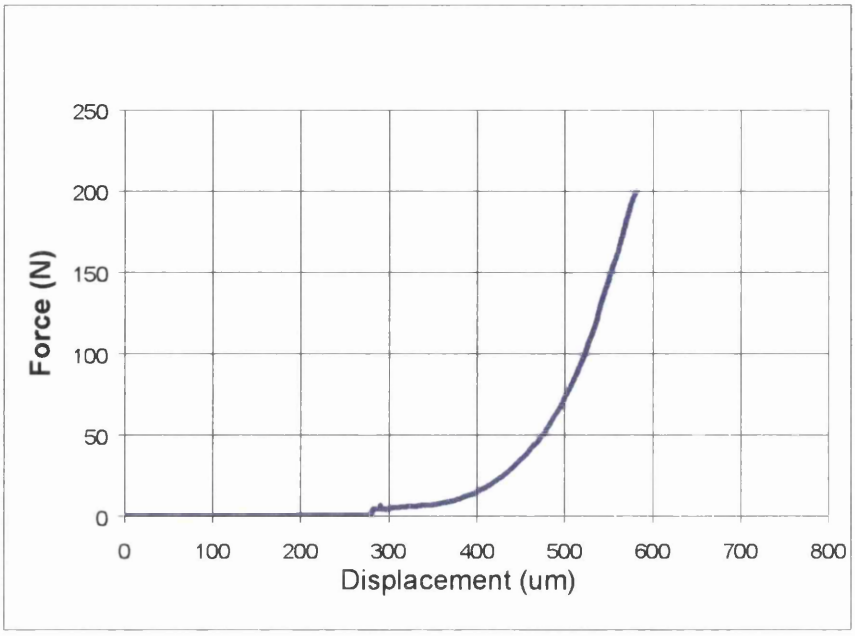

Figure 4.12 – Dynamic Force of 200 N Maximum

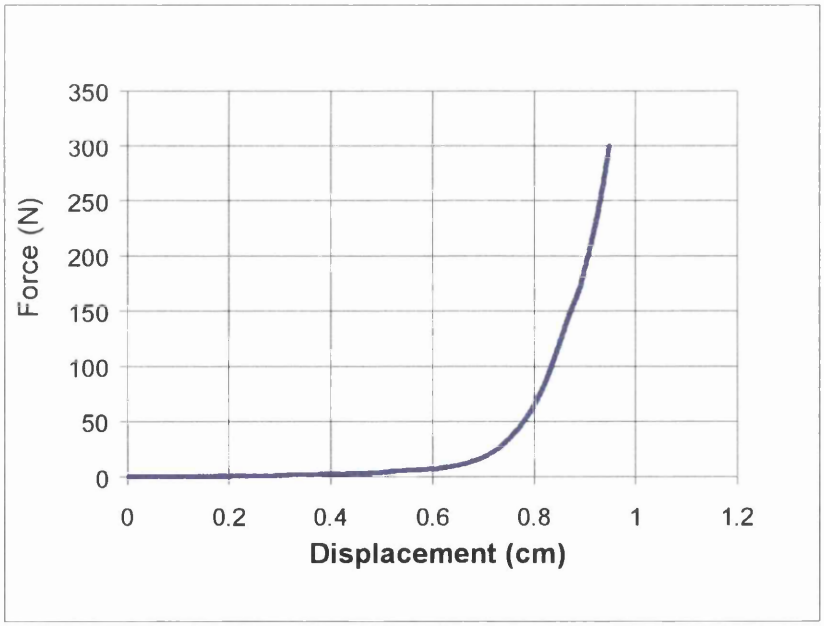

Figure 4.13 – Dynamic Force of 300 N Maximum

4.7 – Electromagnetic susceptibility

Although the electromagnetic interference immunity of optical sensors is stated (Introduction) as one of their attractions for use in sensing system, such claim must be cautiously treated when dealing with polarised light. In fact when an optically isotropic material is introduced into an electromagnetic field, the state of polarisation of the propagating light could be altered, which in turn can modulate the chromaticity. Since the considered optical strain gage is intended to measure force in a potentially hazardous electromagnetic environment, its susceptibility to such effects was considered. Conducting measurement on photoelastic polymers other authors [49] have registered a phase retardation of 1.3×10^{-1} nm using polarised blue light in magnetic fields of 2×10^{3} V/mm. Compared with the retardation experienced by the current gauge (150 nm), this may induce a possible error of (0.13/150) x 100~0.1%. Therefore since the Kerr constant for most plastics is nearly the same, it can be concluded that the susceptibility of the optical strain gauge to electric fields would be sufficiently weak to be neglected.

4.8 - Conclusion

In this Chapter, the basic principle of chromaticity is successfully applied in the development of an optical force sensor. The theory covered in Chapter 3 is applied a to a real challenging Engineering problem. The Sharp PD150 dual photodiode consisting of two diodes with short and long wavelength sensitivities is used to detect the change in the chromaticity, which is in turn proportional to the applied force. The proposed scheme is not dependent on the light intensity and provides total electrical

isolation and immunity to electrical noise, which are problematic in this particular application.

The validity of the proposed optical force sensor is assessed using both the theory and some practical tests. The static test of the proposed optical strain gauge based upon photoelasticity reveals that its response to the applied static force is linear over the range 0-80 N after which it ceases to respond linearly This is consistent with the theory (the transfer function is periodic). The degree of linearity of the output (dominant wavelength) versus the applied force was high and could be further improved using high tolerance of the electronic components and the influence of temperature. The system exhibited a relatively low hysteresis and this could be reduced further by changing the material of the strain gauge but without altering the parameters of the design criteria such as the Young's modulus and strain optic coefficient. Moreover this optical strain gauge shows a considerable resistance to rapidly time varying force, which is of great importance in the pantograph application. It has been also found that the influence of the electric field on the performance characteristic of the optical strain gauge is weak enough to be neglected, and high system repeatability was achieved

CHAPTER 5

FINAL CONCLUSION AND FUTURE WORK

An integrated optical strain gauge based upon photoelasticity is described and tested. The modulation technique used relies upon the chromatic change that can be introduced through the complementary colours generated by variable stress birefringence. This technique has enabled intensity insensitive measurements to be made; therefore a complicated stabilisation technique was not required.

The optical strain gauge consists of a small photoelastic plastic with a suitable Young's modulus and strain optic coefficient fabricated through a casting process to overcome the problems related to the initial birefringence that can be introduced during other process (machining technique). The active area is chosen to be very small to enable the measurement of strain to be made at a point. The linear polariser and the analyser are bonded to the optical fibre launch and receive tips respectively. These fibre tips are cast into the unit, enabling remarkable device ruggedness and overcoming the effects of foreign body ingress.

Light generated by a Tungsten-halogen lamp is injected into a transmitting optical fibre within which it is guided to the sensing area. First this light signal is passed through a linear polariser to convert the incident light into a linearly polarised light. Then, the light signal propagates through the active area where modulation takes place before being re-launched into an exit fibre after passing through an analyser bonded to the front end of the exit fibre.

The transmitting and receiving fibres are connected respectively to the optical source and the detection module by two SMA connectors. To detect the returned spectra, a linear detection technique as described in Chapters 3 and 4 was implemented. The first step of the linear detection technique consists of converting the incident optical signal into two photocurrents by two sequential photodiodes. These two photodiodes have a different but overlapping spectral sensitivity; they correspond to the tristimulus function of the colour spectrum. Then, these two photocurrents are amplified and converted into voltages using transresistance amplifiers. Subsequently, these voltages are fed to a high precision 12-bit ADC,

The proposed optical strain gauge is evaluated and its performance is assessed using both theory and practical tests. In the static test, it was found that the response of the dominant wavelength to the static load is linear over the range of 0 to 80 N. However, the system became non-linear when the applied force exceeded 80 N, it was found that, the same value of wavelength may correspond to different magnitudes of force. This is in agreement with the theory, however, this limits the range of the applied force. This limitation must be taken into account when the proposed system is used in the pantograph application. In addition during the static test, the amount of hysterisis found was small and therefore had no significant effects on the overall performance of the system. One of the most important parameter of interest is the ability of the optical strain gauge to satisfy the repeatability criteria. Extensive tests over a long period of time were carried out and found to have a high degree of repeatability. It was also found and proven by other authors that the influence of electromagnetic interference was negligible.

Dynamic tests were carried out to indicate the resistance of the optical strain gauge to slowly and rapidly varying forces up to 200 N and 300 N. The strain gauge proved

to be resistant to the impact forces, which can be applied in the real pantograph application, where these forces are continuously applied every time the overhead line comes in contact with pantograph head.

All in all the proposed optical strain gauge for pantograph applications is potentially viable and its principle may be used in other industrial applications where conventional transducers cannot be used due to the severe working environment.

Recommendations for Further Work

The following recommendations will be of great benefit to the long-term evaluation of the proposed optical strain gauge:

1. Assess the dynamic performance with the optical strain gauge sensor incorporated into the pantograph and determine the actual bandwidth of the system.
2. Since the pan head of the electric train is subject to a sustained stress, long-term stability of the optical strain gauge should be considered as one or more system components may suffer degradation with time. For example the degradation of the Tungsten–halogen lamp with time may cause a drift in the returned dominant wavelength
3. Since the strain gauge is to be used in a hostile environment, such as high temperature fluctuations, the optical strain gauge needs to be protected from spurious changes of temperature.

REFERENCES

[1]- K.T.V Grattan & B.T Meggitt, 'Optical Fibre Sensor Technology', Chapman & Hall 1995.

[2]- K.T.V Grattan & B.T Meggitt, 'Optical Fibre Sensor Technology', Vol. 2, Devices & Technology, Chapman & Hall 1998.

[3]- John Dakin & Brian Culshaw, 'Optical Fibre Sensor Principles & Components', Vol.1, Artec House 1988.

[4]- M.M Murphy, 'Optical Fibre Structural Monitoring', Phd Thesis, Liverpool University, 1991.

[5]- John Blackwell & Thornton, 'Mastering Optics -An Application Guide To Optical Engineering', Mc Graw Hill 1996.

[6]- Van Etten &Van Der Plaats, 'Fundamentals of Optical Fibre Communications', Prentice Hall 1991.

[7]- C.A Burrus & R.W Dawson, 'Small-Area High-Current-Density GaAs Electroluminescent Diodes And Method of Operation For Improved Degradation Characteristics', Applied Physics Letters, Vol.17, N°.9, 1970.

[8]- Dietrich Marcuse, 'LED Fundamentals: Comparison of Front-and Edge-Emitting Diodes', IEEE Journal of Quantum Electronics, Vol.QE-13, No.10, 1977.

[9]- James P. Wittke, Michael Ettenberg, & Henry, 'High Radiance LED for Surface-Fibre Optical Links', RCVA, Review.37, 1976.

[10]- Klauss Gidersen werner schairer, 'Light Emiting Diodes An Introduction', Prentice Hall, 1987.

[11]- Dan Botez, IEEE Member, And Michael Ettenberg, IEEE Senior Member, 'Comparison of Surface-And Edge-Emitting LED'S For Use In Fibre Optical Communications', Transactions on Electronic Devices, Vol. Ed 26, No.8, 1979.

[12]- Marwood Ediger, 'Electrooptic Handbook', Ronald Waynant, McGraw Hill, 1993.

[13]- A.H Marsden, 'Lamps And Lighting', S.T Henderson, Thorn Lighting Ltd, 1972.

[14]- Gunter Wyszecki W.S.Stiles 'Color Science, Concepts And Methods, Quantitative Data And Formulae, Second Edition, John Willey & Sons, 1982.

[15]- Jeff Heght, 'Understanding Lasers An Entry Level Guide', IEEE Press, 1992.

[16]- J. Wilson, J.F.B Hawkes, 'Lasers-Principles and Applications', Prentice Hall 1987.

[17]- A.E Siegman, 'An introduction to lasers And Masers', McGraw-Hill, 1971.

[18]- Antony E.Siegman, 'Lasers', University Science Books, Mill Valley, California, 1986.

[19]- 'Optical Fibre Communications. Principles And Practice', Second Editions, John Senior, 1992.

[20]- Eli kapon, 'Semiconductor Laser 1 Fundamentals', Academic Press, 1999.

[21]- O.S Heavens & R.W Ditchburn, 'Insight into Optic', John Willey & Sons, 1993.

[22]- Francis T.S.Yu & Xiang Yang, 'Introduction to Optical Engineering', Cambridge University Press, 1997.

[23]- 'Fiber Optic Cables Fundamentals Cable Engineering Systems Planning', John Wiley & Sons limited, 1987.

[24]- D.A. Hill, 'Optical Fibre', 1977.

[25]- D.N Payne & W.A Gambling, 'Zero Material Dispersion in Optical Fibres', Elect-letter.11(8), pp.176-178, 1975.

[26]- F.P.Kapron, D.B.Keck, & R.D.Maurer, 'Radiation Losses In Glass Optical Waveguides', Appl., Phy., Lett. Vol. 17, N^0.10, 1970.

[27]- Masaharu Ohashi, Kazuyuki Shiraki, & Katsusuke Tajman, 'Optical Loss Property Of Silica-Based Single Mode Fibres', Journal of Light wave Technology Vol.10, N°.5, May 1992.

[28]- R. Olshnky, 'Propagation in Glass Optical wave guide', Rev., Mod., Physic., Vol.2, 1979.

[29]- T. Miya, Y. Terunuma, T. Hosaka & T. Miyashita, 'Ultimate Low-Loss Single-Mode Fibre at 1.55 μm', Electronics Letters, Vol.15, N°.4, 1979.

[30]- 'Effect of Dopants on Transmission Loss of Low OH- Content Optical Fibre', Electronic Letter, Vol.12, N°.21, 1976.

[31]- M. Kawachi, A. Kawana & T. Miyashita, 'Low-Loss single mode fibre at the material dispersion free wavelength of 1.27 μm', Electronics Letters, Vol.13, No.15 1977.

[32] D.L Wood, T.Y Kometani, J.P Luongo, & M.A Saifi, 'Incorporation of OH in Glass in the Mcvd Process', Journal of The American Ceramic Society, Vol.62, No.11-12, 1979.

[33]- D.B Keck, R.D Maurer, & P.C Shultz, 'On the Ultimate Lower Limit Of Attenuation In Glass Optical Waveguides'.

[34]- H.Osani, 'Spectral Losses Of Low-OH-Content Optical Fibres', Electronics Letters, Vol.12, No.12, 1976.

[35]- J. Schroeder, R. Mohr, P.B Macedo, & C.J Montrose, 'Rayleigh and Brillouin Scattering in K_2O-S_iO_2 Glasses'.

[36]- Ivan Andonovic & Deepak Uttamchandani, 'Principles Of Modern Optical Systems', Artech House, 1989.

[37]- R.H Stolen, 'Nonlinearity In Fibre Transmission', IEEE Proceeding, 68(10), PP.1232-1236, 1980.

[38]- E.P Ippen , 'Low Power Quasi CW Raman Oscillator', Appl., Phys., Lett., pp.303, 1979,

[39]- R.H Stolen, E.P Ippen, & A.R Tynes, ' Raman Oscillation in Glass Optical Waveguide', Appl., Phys., Letter., Vol.20- 2, 1972.

[40]- E.P Ippen & R.H Stolen, 'Stimulated Brillouin Scattering In Optical Fibres', Appl., Phys., Lett., Vol.21, No.11, 1972.

[41]- S.E Miller & A.G Chynoweth, 'Nonlinear Properties of Optical Fibres', Optical Fibre Telecomunications, pp.125-150, Academic Press, 1979.

[42]- K. Petermann, 'Fundamental Mode Microbending Loss In Graded-Index and W Fibres', Optical and Quantum Electronics, 9, pp.167-179, 1977.

[43]- H.F Wolf , 'Optical waveguides', Handbook of Fibre Optics: Theory and Application, pp.43-152, Granada, 1979.

[44]- M.M Ramsay & G.A Hockhan, 'Propagation in optical waveguides 2', Optical Fibre Communication System, ed. C.P Sandbank, pp.25-41, John Wiley, 1980.

[45]- W.A Gambling, H. Matsumura, & C.M Ragdale, 'Joint Loss In Single-Mode Fibres', Electronic letter, Vol.14, No.15, 1978.

[46]- W.A Gambling, H. Matsumura, A.G Cowley, ' Joint Loss In Single-Mode Fibres', Electronic Letters, Vol.14, No.3, 1978

[47]- Charles Tsao, 'Optical Fibre Wavegude Analysis', Oxford University Press, New York 1992.

[48]- 'Optics. Eugene Hecht', Alfred Zajac Addison-Wesly, Series In Physics, 1974.

[49]- J.P Mathiew, Translated by Professor J. Warren Blaker, 'Optics Part 1 and 2', First edition, 1975.

[50]- Eugene Hecht, 'Theory And Problems Of Optics', McGraw-Hill 1975.

[51]- Allen Nussbaum & Richard A. Phillips, 'Contemporary Optics for Scientists and Engineers', Solid State Physical Electronics Series, Prentice Hall, 1976.

[52]- Francis A. Jenkins. Harvey E. White, 'Fundamentals Of Optics', Fourth Edition McGraw-Hill, 1976.

[53]- Frank L. Pedrotti, S.J & Leno S. Pedrotti, 'Introduction to Optics', Prentice-Hall International, 1987.

[54]- 'The wave Nature Of Light', Prepared By The Science Foundation course Team, The Open University Press, 1971.

[55]- E.H Land, 'Some Aspects of the Development of Sheet Polarizers', J., Opt., Soc., Am.41, 957, 1951.

[56]- R. Wallace Stewart, & John Satterly, Revised by H.N.V Temperley, 'Text Book of Light', M.A. London University Tutorial Press Ltd, 1947.

[57]- D. Clarke T.F Grainger Pergamon, 'Polarised Light and Optical Measurement', Press First Edition 1971.

[58]- 'Polarised Light', William A. Shurcliff & Stanly S. Ballard, A Van Nostrand Company, Inc., 1964.

[59]- Edwin Edser, 'Light For Student', Appendix by N.M. Blich, Macmillan & co, 1944.

[60]- Robert Guenther, 'Modern Optics', John Wiley & Sons, 1990.

[61]-EJ. Hearn Butter Hein Mann, 'Mechanics of materials-2nd edition an introduction to the mechanics of elastic and plastic deformation of solids and structural components', Oxford, Pergamon Press 1977.

[62]- M. M. Frocht, 'Photoelasticity ', Vol.1, John Willey & Son Inc,1941.

[63]- cooker & Filon, 'Photoelasticity', Second Edition, CambridgeUniversity press 1957.

[64]- R.W.Ditchburn, 'Light', third edition, Academic Press, 1979.

[65]- P.S. Theocaris, 'Matrix Theory of Photoelasticity', Vol. 11, Springer-Verlaj, 1979

[66]- A. Kusk & Robertson, 'Photoelastic stress analysis', John Wiley & Sons, 1974.

[67]- H.T Jessop, F.C. Harris, 'Photoelasticity: Principles & Methods', London: Cleaver-Hune Press Ltd, 1949.

[68]- Kings Lake, 'Applied Optics and Optical Engineering - Light its generation and Modulation", Vol.1, academic 1965.

[69]- Society For Experimental Stress Analysis. Educational committee, 'Manual On Experimental Stress Analysis', Edited by W.H Tuppeny, Jr, A.S Kobayashi, Second Edition, Westport, Conn: S.E.S.A, 1965.

[70]- M.M Murphy & G.R Jones, 'Polychromatic Birefringence sensing for Optical Fibre Monitoring of Surface Strain', EUROSENSORS V, 1991.

[71]- M.M Murphy and G.R Jones, 'An extrinsic integrated optical fibre strain sensor', Pure Appl. Opt.2, 1993.

[72]- G.S Halinton, 'Experimental Stress Analysis Principles and Methods', Cambridge University.

[73]- A.W Hendry, 'Elements of Experimental Stress Analysis', SI Edition, Oxford: Pergamon Press, 1977.

[74]-P.J Henderson, J. Spencer and G R Jones,' Pressure sensing using a chromatically addressed diaphragm', Measurement science and technology, 4, 1993.

[75]- G.R Jones, S. Kwan, C. Beavan, P. Henderson, E. Lewis, 'Optical fibre based sensing using chromatic modulation'.

[76]- 'Color Science: Concepts And Methods, Quantitative Data And Formulae', Gunter Wyszecki W.S.Stiles, second Edition.

[77]- D.W. Tenquist, R.M Whittle, J. Yarwood, 'University Optics', Vol.2, 1970.

[78]- S.I. William son & H.Z Cummins, 'Light and Colour in Nature and Art', John Wiley and Sons, 1983.

[79]- D.L. Mac Adam, 'Colour Measurement Theme and Variations', Springer-Verlag, Berlin Heidelberg, New York, 1981.

[80]- Sharp Corporation Electronic Components Group, "Sharp Laser Diodes, User Manual", 22-22 Nagaike-cho, Abeno-ku, Osaka, Japan 1982.

Appendix A

Table A2: Look up Table for 507-1021 nm wavelength readout

Index	Slope*16	Offset
	1.21	1.3
1	0.203593	507.01
2	0.1881226	520.04
3	0.179375	532.08
4	0.172812	543.56
5	0.166563	554.62
6	0.16	565.28
7	0.153281	575.52
8	0.146406	585.33
9	0.139531	594.7
10	0.133125	603.63
11	0.126875	612.15
12	0.121406	620.27
13	0.116406	628.04
14	0.111719	635.49
15	0.107812	642.64
16	0.104063	649.54
17	0.100937	656.2
18	0.0981255	662.66
19	0.956249	668.94
20	0.0934372	675.06
21	0.0914068	681.04
22	0.0898438	686.89
23	0.0884371	692.64
24	0.0871878	698.3
25	0.0860939	703.88
26	0.0853119	709.39
27	0.0846882	714.85
28	0.0840626	720.27
29	0.0837498	725.65
30	0.0835934	731.01
31	0.0834379	736.36
32	0.0831251	741.7
33	0.0837498	747.02
34	0.0840626	752.38
35	0.0846872	757.76
36	0.08515664	763.18
37	0.0859375	768.63
38	0.086875	774.13
39	0.0878124	779.69
40	0.0892191	785.31
41	0.0904684	791.02
42	0.0920315	796.81
43	0.0939064	802.7
44	0.0957813	808.71

45	0.0892191	814.84
46	0.10047	821.1
47	0.102968	827.53
48	0.109375	834.12
49	0.10047	840.91
50	0.113126	847.91
51	0.117188	855.15
52	0.121718	862.65
53	0.127031	870.44
54	0.132812	878.57
55	0.139375	887.07
56	0.147032	895.99
57	0.155781	905.4
58	0.166094	915.37
59	0.178125	926
60	0.193125	937.4
61	0.212031	949.76
62	0.238593	963.33
63	0.281095	978.6
64	0.386093	996.59

Appendix B

C Program Flow Chart

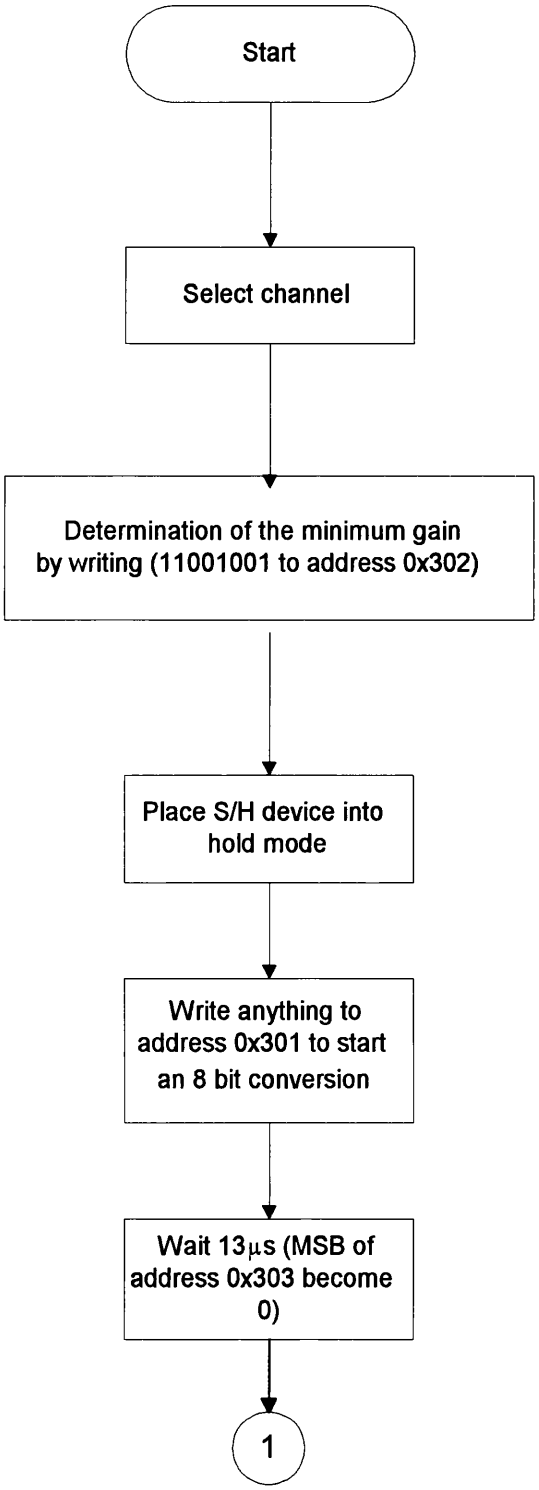

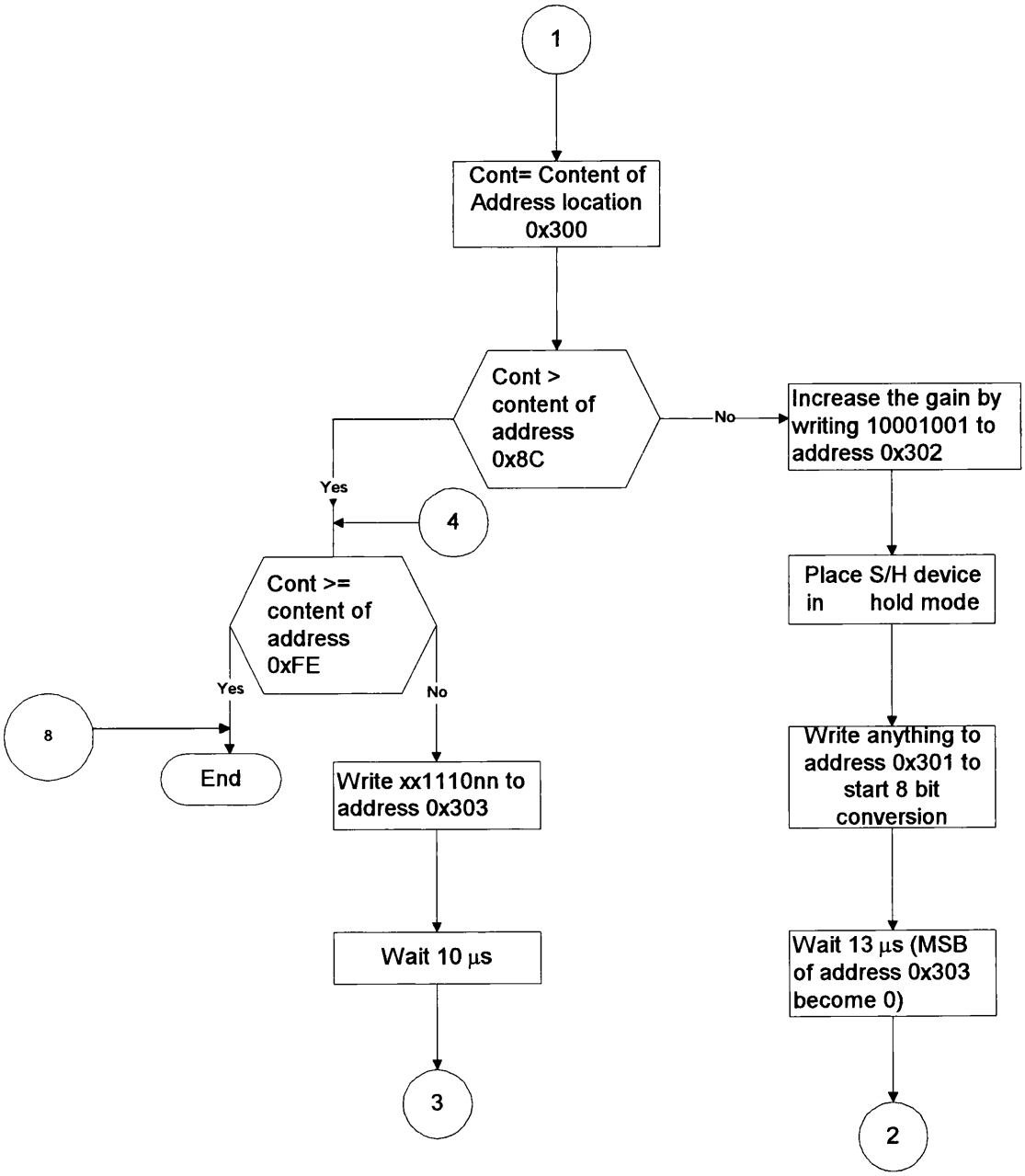
1
Cont= Content of Address location 0x300
Cont > content of address 0x8C
No
Increase the gain by writing 10001001 to address 0x302
Yes
4
Cont >= content of address 0xFE
Yes
No
8
End
Write xx1110nn to address 0x303
Wait 10 μs
3
Place S/H device in hold mode
Write anything to address 0x301 to start 8 bit conversion
Wait 13 μs (MSB of address 0x303 become 0)
2

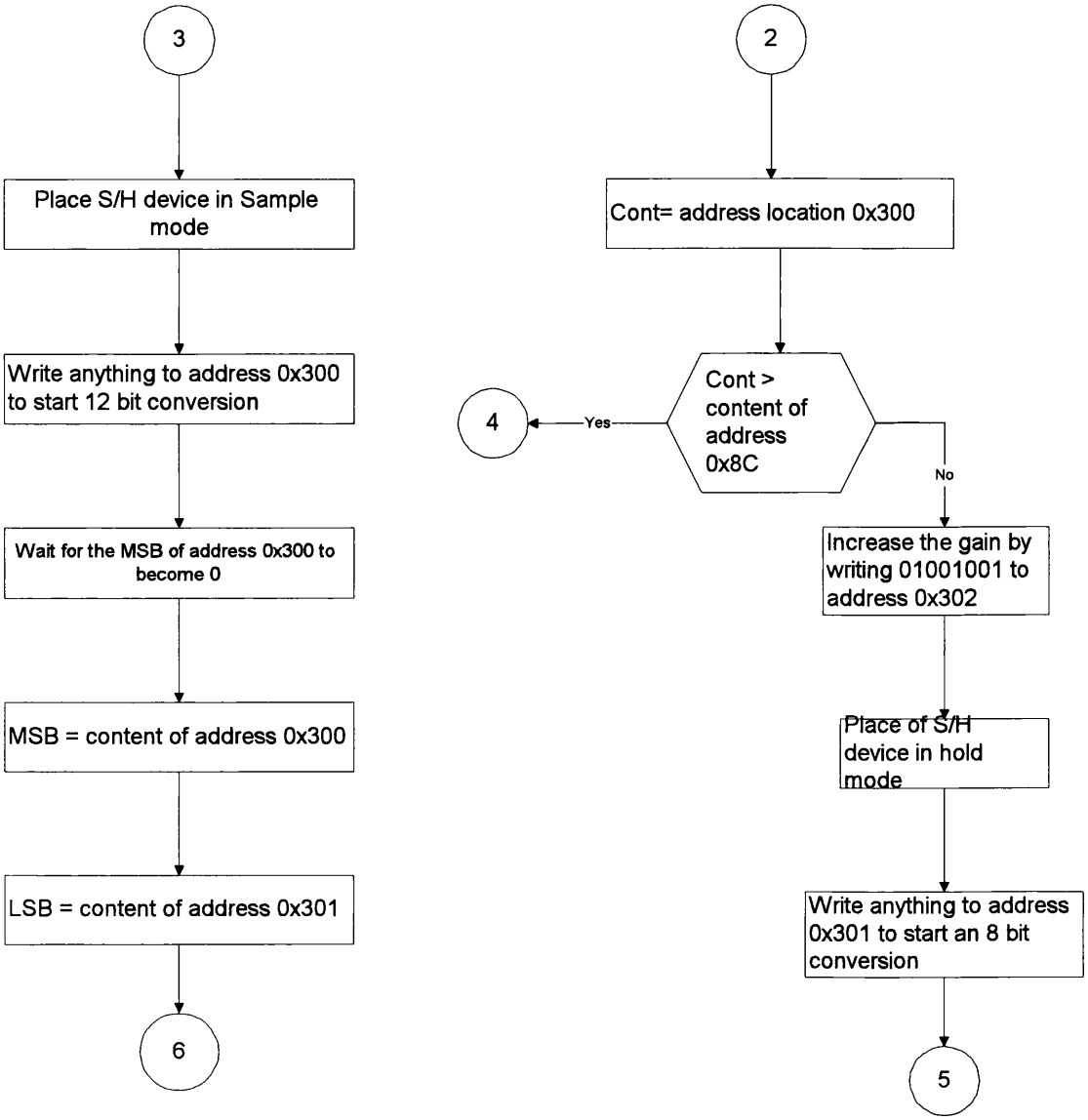
3
Place S/H device in Sample mode
Write anything to address 0x300 to start 12 bit conversion
Wait for the MSB of address 0x300 to become 0
MSB = content of address 0x300
LSB = content of address 0x301
6
2
Cont= address location 0x300
Cont > content of address 0x8C
Yes
4
No
Increase the gain by writing 01001001 to address 0x302
Place of S/H device in hold mode
Write anything to address 0x301 to start an 8 bit conversion
5

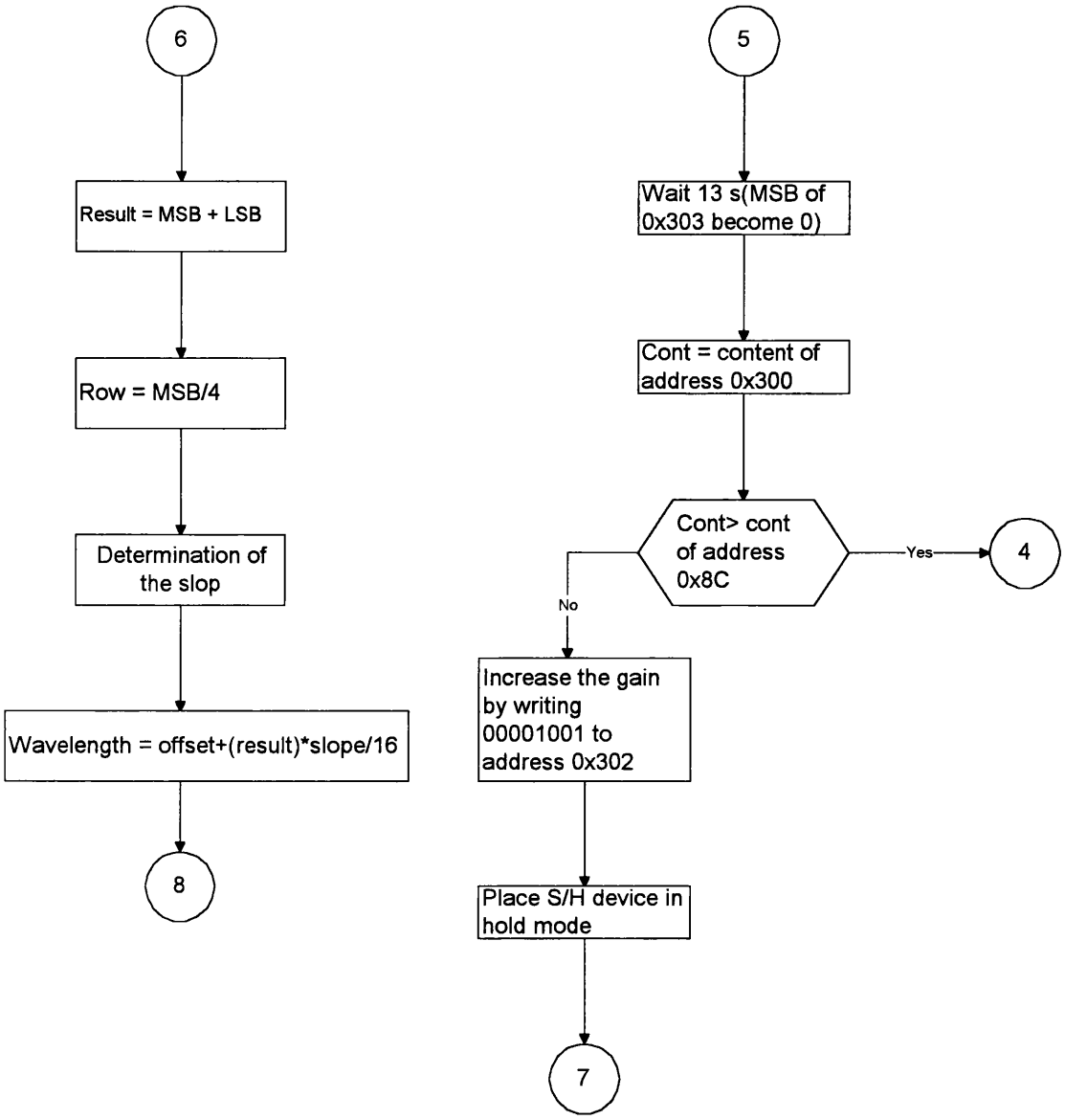
6
Result = MSB + LSB
Row = MSB/4
Determination of the slop
Wavelength = offset+(result)*slope/16
8
5
Wait 13 s(MSB of 0x303 become 0)
Cont = content of address 0x300
Cont> cont of address 0x8C
Yes
4
No
Increase the gain by writing 00001001 to address 0x302
Place S/H device in hold mode
7

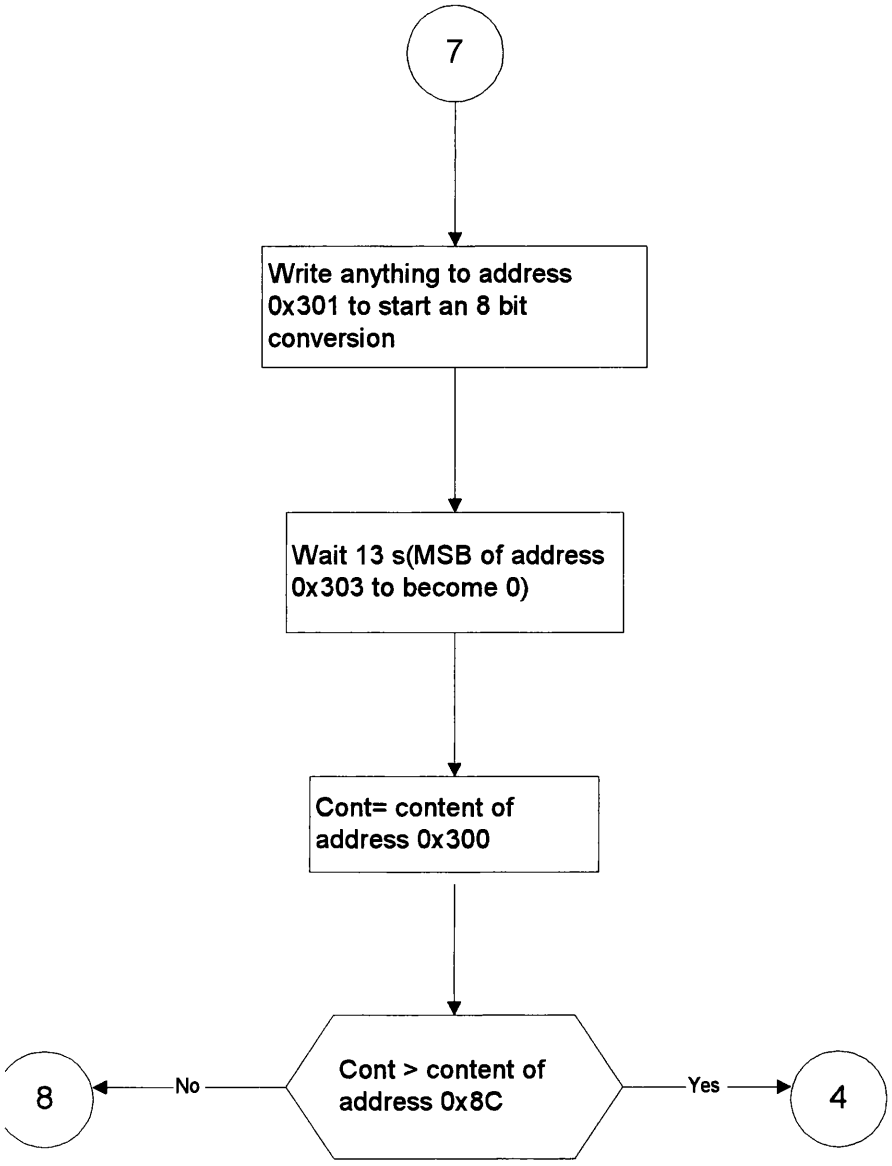
7
Write anything to address 0x301 to start an 8 bit conversion
Wait 13 s(MSB of address 0x303 to become 0)
Cont= content of address 0x300
Cont > content of address 0x8C
No
Yes
8
4